CHAPTER 19
JOURNAL BEARINGS

Theo G. Keith, Jr., Ph.D.
Professor and Chairman of Mechanical Engineering
University of Toledo
Toledo, Ohio

LIST OF SYMBOLS

a	Axial-flow land width
a_f	Pad load coefficient
A	Area
b	Circumferential-flow land width
C	Clearance
C^*	Specific heat
D	Diameter
e	Eccentricity
f	Coefficient of friction
F_j	Friction on journal
h	Film thickness
h_0	Minimum film thickness
H	Dimensionless film thickness
J	Mechanical equivalent of heat
k	Permeability
L	Bearing width
M	Rotor mass at bearing
M_j	Frictional torque on journal

n	Number of pads or recesses
N	Revolutions per unit time
p	Pressure
p_a	Ambient pressure
p_0	Short-bearing pressure
p_r	Recess pressure
p_s	Supply pressure
p_∞	Long-bearing pressure
$\overline{p}$	Dimensionless pressure
P	Unit loading
q	Volume flow rate per unit length
q_f	Flow factor
Q	Volume flow rate
Q_s	Side leakage flow rate
R	Radius of journal
R_b	Radius of bearing = $R + C$
s	Stiffness
S	Sommerfeld number = $(\mu N/P)(R/C)^2$
t	Time
t_p	Thickness of porous liner
T	Temperature
u, v, w	Velocity in x, y, z directions, respectively
U	Velocity of journal
W	Load
W_R	Load component directed along line of centers
W_T	Load component normal to line of centers
x, y, z	Rectangular coordinates
X	Dimensionless minimum-film-thickness parameter = $(h_0/R)[P/(2\pi N\mu)]^{1/2}$
Y	Dimensionless frictional torque parameter = $[M_j/(WR)][P/(2\pi N\mu)]^{1/2}$
α	Porous material slip coefficient
β	Included angle of partial bearing, porous bearing parameter
β_1	Angle from line of centers to leading edge of partial bearing
γ	Circumferential-flow parameter
ε	Eccentricity ratio e/c
ζ	Dimensionless axial dimension = $z/(L/2)$
θ	Angular position measured from line of centers
θ_1	Angular position to leading edge of film
θ_2	Angular position to zero pressure in film
θ_3	Angular position to trailing edge of film
θ_{cav}	Angular position to cavitation boundary

Λ	Bearing number = $(6\mu\omega/p_a)(R/C)^2$
λ	Ratio of heat conduction loss to heat generation rate, reduced bearing number = $\Lambda/6$
μ	Dynamic viscosity
ρ	Density
τ	Shear stress
ϕ	Attitude angle
ω	Angular velocity
Ω	Porous bearing parameter

19.1 INTRODUCTION

The design of journal bearings is of considerable importance to the development of rotating machinery. Journal bearings are essential machine components for compressors, pumps, turbines, internal-combustion engines, motors, generators, etc.

In its most basic form (Fig. 19.1), a *journal bearing* consists of a rotatable shaft (the journal) contained within a close-fitting cylindrical sleeve (the bearing). Generally, but not always, the bearing is fixed in a housing. The journal and bearing surfaces are separated by a film of lubricant (liquid or gas) that is supplied to the *clearance* space between the surfaces. The clearance space is generally quite small (on the order of one-thousandth of the journal radius) and has four major functions:

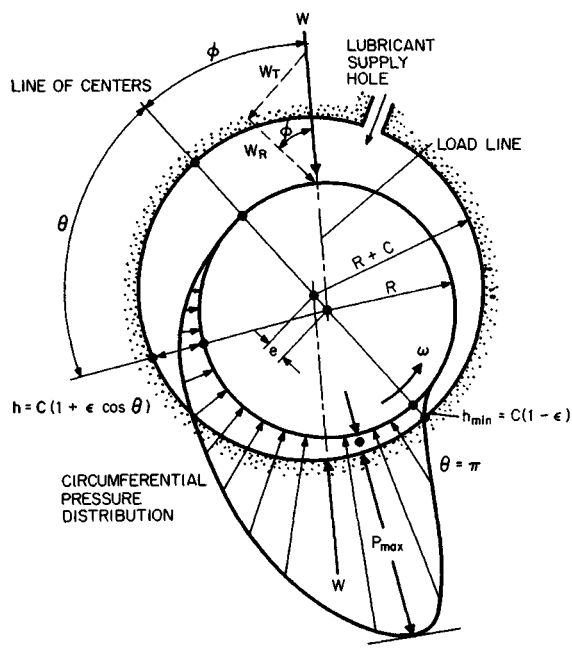

FIGURE 19.1 Journal and bearing notation.

to permit assembly of the journal and bearing, to provide space for the lubricant, to accommodate unavoidable thermal expansions, and to tolerate any shaft misalignment or deflection.

The fundamental purpose of a journal bearing is to provide radial support to a rotating shaft. Under load, the centers of the journal and the bearing are not coincident but are separated by a distance called the *eccentricity.* This eccentric arrangement establishes a converging-wedge geometry which, in conjunction with the relative motion of the journal and the bearing, permits a pressure to be developed by viscous effects within the thin film of lubricant and thus produces a load-carrying capability. However, if the load is too large or the shaft rotation too slow, the wedge-like geometry will not form and solid-to-solid contact can occur.

Journal bearings can operate in any of three lubrication regimes: *thick-film lubrication, thin-film lubrication,* or *boundary lubrication.* Generally, thick-film operation is preferred. Figure 19.2 is a diagram of the three lubrication regimes. Table 19.1 provides some of the characteristics of each regime.

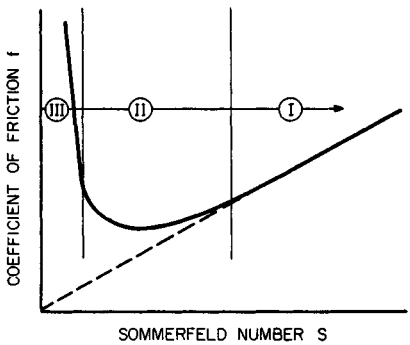

FIGURE 19.2 Three lubrication regimes: I, thick film; II, thin film; III, boundary.

Journal bearings may be classified according to the fluid mechanism that establishes the film load capacity: *Hydrodynamic* journal bearings, also called *self-acting* bearings, depend entirely on the relative motion of the journal and the bearing to produce film pressure for load support. *Hydrostatic* journal bearings, also called *externally pressurized* bearings, achieve load support by the supply of fluid from an external high-pressure source and require no relative motion between journal and bearing surfaces. *Hybrid* journal bearings are designed to use both hydrodynamic and hydrostatic principles to achieve load support between moving surfaces.

19.2 BEARING AND JOURNAL CONFIGURATIONS

19.2.1 Bearing Geometries

A wide range of bearing configurations are available to the journal bearing designer. Figure 19.3 depicts several of these bearings. The configurations range from the very simple plain journal bearing to the very complex tilting-pad bearing. The choice of bearing configuration depends on several factors. Among the more important are cost, load, power loss, dynamic properties, ease of construction, and difficulty of installation.

Journal bearings are termed *full bearings* (Fig. 19.3*a*) when the bearing surface completely surrounds the journal. Because they are easy to make and do not cost much, full bearings are the most commonly used bearing in rotating machinery. Full bearings become distorted during installation, and so they are generally not perfectly circular.

Journal bearings are called *partial bearings* when the bearing surface extends over only a segment of the circumference, generally 180° or less (Fig. 19.3*b*). Par-

TABLE 19.1 Characteristics of Lubrication Regimes

Lubrication regime	Contact of bearing surfaces	Range of film thickness, in	Coefficient of friction	Degree of wear	Comments
Thick film	Only during startup or stopping	10^{-3}–10^{-4}	0.01–0.005	None	1. Light-loading high-speed regime 2. Friction coefficient proportional to $\mu N/[W/(LD)]$
Thin film	Intermittent; dependent on surface roughness	10^{-4} to 0.5×10^{-4}	0.005–0.05	Mild	1. High operating temperatures
Boundary	Surface to surface	0.5×10^{-4} to molecular thicknesses	0.05– 0.15	Large	1. Heavy-loading (unit load > 3000 psi) low-speed (< 60 fpm) operating regime 2. Heat generation and friction not dependent on lubricant viscosity

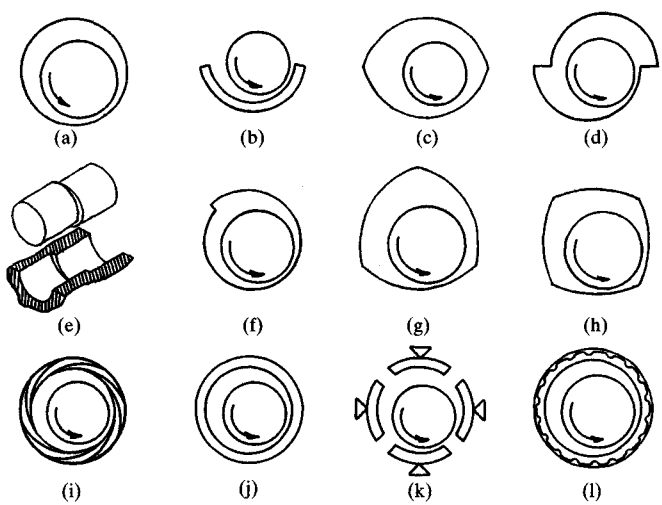

FIGURE 19.3 Journal bearing geometries. (*a*) Full bearing; (*b*) partial bearing; (*c*) elliptical, or lemon, bearing; (*d*) offset bearing; (*e*) rocking journal bearing; (*f*) pressure dam bearing; (*g*) three-lobe bearing; (*h*) four-lobe bearing; (*i*) multileaf bearing; (*j*) floating-ring bearing; (*k*) tilting- or pivoted-pad bearing; (*l*) foil bearing.

tial bearings are used in situations where the load is mainly unidirectional. Partial journal bearings have been found to reduce frictional torque on the journal and provide convenient accessibility, and they do not, in many instances, require strict manufacturing tolerance. Partial journal bearings in which the bearing radius exceeds the journal radius are called *clearance bearings,* whereas partial journal bearings in which the bearing and the journal radii are equal are termed *fitted bearings.*

Geometries in which two circular sectors are employed are called *elliptical,* or *lemon, bearings* (Fig. 19.3*c*). These bearings are really not elliptical at all but are fabricated by uniting two halves of a circular bearing which have had their mating faces machined so that the bearing has an approximately elliptical appearance. Lemon bearings are probably the most widely used bearings at low and moderate speeds. They are extensively used in turbine applications.

Elliptical bearings in which the two cylindrical halves are laterally displaced along the major axis are termed *offset bearings* (Fig. 19.3*d*). The relative displacement of the center of each half of the bearing is called the *preset.* When the upper half of the bearing is displaced horizontally in the direction of rotation, the bearing has negative preset. It is found that load capacity increases with preset. Offset bearings have relatively high horizontal stiffness, which helps prevent dynamic instability. Further, offset bearings allow greater lubricant flow and so run cooler.

Novel offset journal bearing designs for reducing power loss and wear in duty cycles which combine nonreversing loading with limited journal angular oscillation or in steady operation with counterrotation of journal and bearing under a constant load have been studied. In these applications, conventional journal bearings are found to develop extremely thin lubricant films, which in turn results in high friction and wear. Figure 19.3*e* depicts a journal bearing in which both the journal and the bearing are divided axially into segments with offset centerlines. This arrangement produces a dynamic rocking motion which promotes a thicker lubricating film. Accordingly the assembly has been called a *rocking journal bearing.*

When a step is milled from the surface of the bearing (Fig. 19.3*f*), the resulting bearing is called a *pressure dam,* or *step, bearing.* The purpose of the step is to create additional hydrodynamic pressure on the top of the journal as the lubricant is rotated into the step. In turn, this pressure buildup enhances the load on the journal and therefore diminishes its susceptibility to vibration problems. Pressure dam bearings are very popular in the petrochemical industry.

Bearing geometries consisting of three or more sectors (Fig. 19.3*g* and *h*) are termed *lobed,* or *multilobed, bearings.* Generally, bearings with more than three lobes are used only in gas bearing applications. Multilobed bearings act as a number of partial bearings in series. The cost of multilobed bearings is considered moderate.

The *multileaf journal bearing* (Fig. 19.3*i*) is a variant of a multilobed bearing. It consists of a number of identical circular arcs, or leaves, whose centers are equally spaced around the generating circle. The operating characteristics of a multileaf bearing are practically independent of the direction of loading for bearings with eight or more leaves.

In a *floating-ring journal bearing* (Fig. 19.3*j*), the lubricating film is divided in two by the addition of a "floating" ring between the journal and the bearing. Floating-ring bearings have lower frictional losses and reduced heat generation and provide better stability.

Hydrodynamic journal bearings may be distinguished by whether the bearing surface can pivot. The basic advantage of *pivoting,* or *tilting-pad, journal bearings* (Fig. 19.3*k*) over fixed-pad journal bearings is that they can accommodate, with little loss in performance, any shaft deflection or misalignment.

A *foil journal bearing* (Fig. 19.3*l*) consists of a very thin compliant bearing surface resting atop a series of corrugations. When it is compared to a conventional gas bearing, the foil bearing has a thicker film, higher load capacity, lower power loss, better stability, and superior endurance to high operating temperatures.

19.2.2 Journal Shapes

Although the journal is generally assumed to be perfectly circular, wear effects or poor manufacture can lead to journals with the shapes shown in Fig. 19.4*a, b,* and *c.* In addition, the possibility of developing pressure by grooving the surface of the journal has been investigated. Three grooved patterns that were found to yield good stability characteristics are shown in Fig. 19.4*c, d,* and *e.*

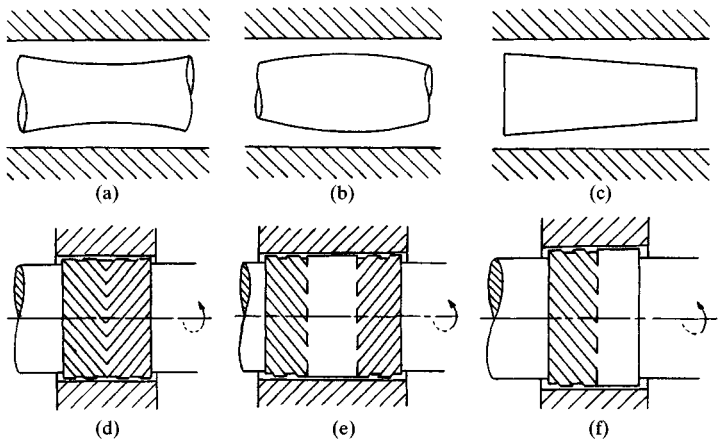

FIGURE 19.4 Journal shapes. (*a*) Hourglass; (*b*) barrel; (*c*) tapered; (*d*) herringbone; (*e*) partly grooved symmetrical pattern: (*f*) partly grooved asymmetrical pattern. *(Parts (d), (e), and (f) are from [19.1].)*

19.3 BEARING MATERIALS AND SELECTION CRITERIA

19.3.1 Bearing Materials

The ideal journal bearing material would have the following characteristics:

1. High compressive strength to withstand the applied radial loading
2. High fatigue strength to endure any cyclic changes in load direction and/or load intensity
3. Compatibility with the journal material to minimize surface scoring and bearing seizure whenever the journal and bearing surfaces come into contact (e.g., during startup)
4. Embedability to permit foreign particles in the lubricant to penetrate the bearing surface to avoid scoring and wear

5. Conformability of surface to tolerate journal misalignment, deflection, or manufacturing inaccuracies
6. High corrosion resistance to withstand chemical attack by the lubricant
7. High thermal conductivity to permit generated heat to be transported from the lubricant film
8. Appropriate coefficient of thermal expansion to avoid differences in thermal expansion of the journal and bearing
9. Low wear to prevent surface destruction, especially under boundary lubrication conditions (i.e., thin-film high-friction lubrication), and thereby lengthen the life of the bearing

Besides all these, the material should be inexpensive, highly available, and easily machined.

To be sure, no single material has been developed that satisfactorily combines all characteristics of the ideal bearing material. In fact, some of the characteristics are contradictory. For example, soft bearing materials generally do not have sufficient strength. To strengthen soft bearing materials, they are frequently bonded to stronger backing materials. Bearing linings or overlays may be cast, electrodeposited, sprayed, or chemically applied, and they have thicknesses which range from 0.01 to 0.5 inch (in).

Journal bearing materials may be broadly divided into two groups: metallics and nonmetallics. The metallic group includes aluminum alloys, babbitts (tin-, lead-, and aluminum-based), copper alloys (brass and bronze), zinc, and iron. The nonmetallic group includes plastics, carbon graphites, cemented carbides, and other proprietary materials. The nonmetallics have been widely used in self-lubrication applications because they can provide low friction and wear without the aid of a lubricant.

Because of the wide diversity of materials available for use in journal bearings, it is difficult to provide comprehensive tables of all relevant properties. Manufacturers and materials suppliers are the best sources for that information. Nevertheless, some physical properties of a variety of journal bearing materials are presented in Table 19.2 [19.2]. Typical applications and useful comments concerning a number of journal bearing alloys are displayed in Table 19.3, while Table 19.4 contains a numerical ranking of the performance characteristics of these alloys.

General information for a variety of self-lubricating materials is given in Table 19.5 [19.3]. Note that the table contains maximum values of the PV factor. This factor is the product of the bearing load per unit of projected area and the sliding velocity (i.e., speed in revolutions per minute times the bearing circumference). The PV parameter provides an indication of material wear and internal heat generation. Failure in self-lubricated bearings is frequently the direct result of internal overheating.

19.3.2 Bearing Material Selection Criteria

Selection of a bearing material invariably requires a compromise based on particular characteristics regarded by the designer to be of principal importance to the application at hand. DeGee [19.4] has developed a systematic approach for selecting a material for lubricated journal bearings. In this method, certain component criteria are identified within major property groups. Table 19.6 gives one such listing.

Not all the criteria presented in Table 19.6 need be considered. For example, in a particular application, environmental properties may be of no concern because the

TABLE 19.2 Physical Properties of Journal Bearing Materials

Material	Hardness H_B	Tensile strength, kpsi	Modulus of elasticity, Mpsi	Thermal conductivity, Btu/(h·ft·°F)	Coefficient of expansion, μin/(in·°F)	Density, lbm/ft³
Metals						
Lead babbitt	21	10	4.2	14	14	630
Tin babbitt	25	11	7.6	32	13	462
Copper lead	25	8	7.6	170	11	562
Silver	25	23	11	238	10.9	655
Cadmium	35	....	8	53	16.6	537
Aluminum alloy	45	22	10.3	119	13.5	181
Lead bronze	60	34	14	27	9.9	555
Tin bronze	70	45	16	29	10	549
Steel	150	75	30	29	6.4	487
Cast iron	180	35	23	30	5.7	449
Porous metals						
Bronze	40	18	....	17	10.5	399
Iron	50	25	....	16	6.7	381
Aluminum	H55†	15	....	....	....	144
Plastics						
TFE	D60‡	3	0.06	0.10	55	137
Nylon	M79†	11	0.41	0.14	55	71
Phenolic	M100	10	0.5	0.21	12	85
Acetal	M94	10	0.41	0.13	45	89
Polycarbonate	M70	8.5	0.32	0.11	70	75
Filled polyimide	E99†	7.5	....	0.44	22	89
Other nonmetallics						
Rubber	....	....	....	0.09	43	75
Wood	....	1.1	1.8	0.11	2.7	42
Carbon graphite	75§	2	2	10	1.5	106
Cemented tungsten carbide	A91†	130	81	40	3.3	886
Fused aluminum oxide	A85	30	50	1.6	8.2	243

†Rockwell. ‡Shore durometer. §Shore scleroscope.

SOURCE: Ref. [19.2].

TABLE 19.3 Bearing Alloy Material Applications

Material	Nominal composition, % by weight	Applications and remarks
Aluminum, low tin	Al 92 Sn 8	Tin added to improve compatibility; too much tin lowers strength. Has thermal expansion problems in steel housings. Requires hard journals. Good at high temperatures. Used in diesel engines and compressors.
Aluminum, high tin	Al 80 Sn 20	Produced by special working and annealing process so tin content does not greatly reduce strength. Used in automotive engines (crankshafts) and in aircraft equipment.
Babbitt, tin-based	Sn 84 Cu 8 Sb 8	Fatigue strength decreases as thickness increases. Low load capacity, thus usually bonded to one (bimetal) or two (trimetal) backing materials. Good in dirty applications, motors.
Babbitt, lead-based	Pb 75 Sn 10 Sb 15	Antimony (Sb) greater than 15% can cause brittleness. Cheaper than tin-based babbitt. Used in crankshaft bearings, transmission bushings, and electric equipment.
Lead bronze	Cu 70 Pb 25 Sn 5	Good for high-load high-speed applications; can be used with soft journals. Used as bushings in pumps, many home appliances, railroad cars.
Phosphor bronze	Cu 80 Sn 10 Pb 10	General-duty popular bushing; tin added to improve strength. Has high hardness; should be used with harder journals (300 BHN). Good impact resistance; used in lathes, pumps, home appliances.
Copper lead (cast)	Cu 75 Pb 25	Lead in pockets in copper matrix. Lead improves bearing surface but has corrosion problems. Frequently used as lining material on steel-backed bearings. Used in heavy-duty applications.
Copper lead (sintered)	Cu 75 Pb 25	Frequently used with a babbitt overlay in a trimetal bearing. Widely used in heavy-duty (high-temperature high-load) applications.
Silver (oven-plated)		Frequently used with lead indium overlay.

bearing operates in a clean, moderate-temperature environment and is not part of an electric machine.

After the list of criteria has been established, each component criterion is compared with all other criteria, and a graduation mark is allocated from 0, if there is no difference in the criterion, to 3, if there are large differences. For example, compressive strength (A1 in Table 19.6) might receive a 0 when compared with fatigue strength (A2) but receive a 3 when compared to thermal conductivity (B1), and so forth. When all component criteria have been compared with one another and graduation marks assigned, the graduation marks of each criterion are totaled and the sum of all these totals is divided into each amount, to obtain the component criteria weighting factors. The sum of all the weighting factors obviously is unity.

TABLE 19.4 Performance Ratings from 5 (High) to 1 (Low) for Bearing Alloy Materials

Material	Nominal composition, % by weight	Fatigue strength	Corrosion resistance	Seizure resistance	Embedability	Compatibility	Thermal conductivity
Aluminum, low tin	Al 92 Sn 8	2	4	2	1	1	4
Aluminum, high tin	Al 80 Sn 20	2	4	2	2	2	4
Babbitt, tin-based	Sn 84 Cu 8 Sb 8	1	5	4	5	4	3
Babbitt, lead-based	Pb 75 Sn 10 Sb 15	1	3	4	5	4	2
Lead bronze	Cu 70 Pb 25 Sn 5	4	2	3	3	2	3
Phosphor bronze	Cu 80 Sn 10 Pb 10	4	2	3	1	2	3
Copper lead (cast)	Cu 75 Pb 25	3	1	3	3	3	4
Copper lead (sintered)	Cu 60 Pb 40	3	1	3	3	3	4
Silver (over-plated)		5	4	1	1	1	5

TABLE 19.5 General Information on Self-Lubricating Bearing Materials

Material	Maximum load,† kpsi	Maximum speed, fpm	Maximum *PV* factor,‡ kpsi·fpm	Friction coefficient	Critical temperature, °F	Resistance to humidity	Resistance to chemicals§
Nylon	1.5	200–400	1	0.1–0.4	400	Fair	Good
Acetal	1.5	200–500	1	0.1–0.4	300	Good	Good
Polyimide	10	1000	0.3	0.1–0.3	600	Good	Good
Phenolic	4	1000	0.1	0.9–1.1	300–400	Good	Good
Filled nylon	2	200–400	1	0.1–0.4	400	Fair	Good
Acetal PTFE filled	1.8	800	2.5	0.05–0.15	300	Good	Good
Filled polyimide	10	1000	6	0.1–0.3	600	Good	Good
Reinforced phenolic	4–5	200	4	0.1–0.4	300–400	Good	Good
Filled PTFE	1	500–1000	5–20	0.05–0.25	500	Excellent	Excellent
PTFE	100	50	1–10	0.05–0.25		Excellent	Excellent

†Load on projected area at zero speed.
‡For continuous service.
§At bearing surface.
SOURCE: Ref. [19.3].

TABLE 19.6 Journal Bearing Material Selection Criteria

Major property group	Component criteria
A. Mechanical	1. Compressive strength 2. Fatigue strength 3. Conformability (modulus of elasticity)
B. Thermal	1. Thermal conductivity 2. Thermal expansion
C. Chemical	1. Corrosion rate
D. Manufacturing	1. Cost 2. Machinability 3. Availability of material
E. Environmental	1. Behavior under abrasive conditions (embedability) 2. Resistance against electric-discharge pitting 3. Resistance to thermal degradation
F. Tribological	1. Wear rate 2. Coefficient of friction 3. Cavitation erosion resistance

Next the candidate materials are given quality marks for the various component criteria. These marks range from 5 (excellent, or high) to 1 (poor, or low). For instance, tin-based babbitts are known to have only fair (2) fatigue strength, whereas they have excellent (5) resistance to corrosion. The final ranking of the candidate materials is obtained by comparing the sums of the products of all component criteria weighting factors and quality marks.

19.4 PRESSURE EQUATION FOR A LUBRICATING FILM

19.4.1 Reynolds Equation

The differential equation which governs the pressure in a lubricating film is called the *Reynolds equation.* Bearing performance can be evaluated once the solution of this equation is in hand.

To develop the Reynolds equation, consider a portion of the fluid film of a journal bearing (Fig. 19.1). In general, there are three velocity components in the film: u, v, and w. There are three equations of motion (momentum equations), one for each coordinate direction. The collection is known as the *Navier-Stokes equations,* and each equation may be written in the following form:

$$\text{Inertial forces} = \text{pressure forces} + \text{body forces} + \text{viscous forces} \qquad (19.1)$$

The Navier-Stokes equations in their complete form are too involved for analytical solution. They can, however, be reduced, and subsequently solved, by making several simplifying yet plausible assumptions:

1. The flow is laminar.
2. The inertial and body forces are small compared to the pressure and viscous forces.
3. The curvature of the film is negligible; the bearing surfaces are, therefore, nearly parallel.
4. The variation of pressure across the film $\partial P/\partial y$ is negligibly small.
5. The transverse velocity component across the film, v, is small compared to the other velocity components.
6. The velocity gradients across the film dominate over all other velocity gradients.

Application of these assumptions to mathematical versions of Eq. (19.1), and to an integrated version of the conservation of mass (the continuity equation), yields the *Reynolds equation* for a liquid-lubricated bearing:

$$\frac{\partial}{\partial x}\left(\frac{h^3}{\mu}\frac{\partial p}{\partial x}\right)+\frac{\partial}{\partial z}\left(\frac{h^3}{\mu}\frac{\partial p}{\partial z}\right)=6(U_b+U_j)\frac{\partial h}{\partial x}+6h\frac{\partial(U_b+U_j)}{\partial x}+12\frac{\partial h}{\partial t} \tag{19.2}$$

The first grouping on the right-hand side of Eq. (19.2) is called the *wedge* term and must be negative to generate positive pressures. The third term on the right is called the *squeeze* term, and it will generate positive pressures when $\partial h/\partial t < 0$. The squeeze term vanishes for a steadily loaded bearing. Both the wedge and the squeeze terms vanish for a purely hydrostatic case. If the bearing surface is fixed ($U_b = 0$), if the shaft is rotating with a speed ω (that is, $U_j = U = R\omega$), and if the viscosity of the lubricant is constant, then Eq. (19.2) may be written as

$$\frac{\partial}{\partial x}\left(h^3\frac{\partial p}{\partial x}\right)+\frac{\partial}{\partial z}\left(h^3\frac{\partial p}{\partial z}\right)=6\mu R\omega\frac{\partial h}{\partial x}+6\mu h\frac{\partial U}{\partial x}+12\mu\frac{\partial h}{\partial t} \tag{19.3}$$

For comparative purposes, it is useful to cast the steady version of Eq. (19.3) into nondimensional form. This can be accomplished by defining the following nondimensional variables:

$$\theta\equiv\frac{x}{R}\qquad\zeta\equiv\frac{z}{L/2}\qquad H\equiv\frac{h}{C}$$

$$\bar{p}\equiv\frac{p}{6\mu(U/R)}\left(\frac{C}{R}\right)^2=\frac{p}{6\mu\omega}\left(\frac{C}{R}\right)^2$$

Also, since $\omega = 2\pi N$,

$$\bar{p}=\frac{p}{12\pi\mu N}\left(\frac{C}{R}\right)^2$$

Substituting these into Eq. (19.3) yields

$$\frac{\partial}{\partial\theta}\left(H^3\frac{\partial\bar{p}}{\partial\theta}\right)+\left(\frac{D}{L}\right)^2\frac{\partial}{\partial\zeta}\left(H^3\frac{\partial\bar{p}}{\partial\zeta}\right)=\frac{\partial H}{\partial\theta} \tag{19.4}$$

This equation can be interpreted as

Circumferential pressure flow + axial pressure flow = shear flow

The governing equation of a gas film differs from that of a liquid film by the appearance of the *density* ρ. The steady compressible version of the Reynolds equation for an isoviscous gas can be written

$$\frac{\partial}{\partial x}\left(h^3\rho\frac{\partial p}{\partial x}\right)+\frac{\partial}{\partial z}\left(h^3\rho\frac{\partial p}{\partial z}\right)=6\mu R\omega\frac{\partial(\rho h)}{\partial x} \tag{19.5}$$

Since the energy dissipated by frictional forces is very small in normal gas bearing operation, we may assume that the film has a constant temperature and $p = k\rho$; thus, Eq. (19.5) becomes

$$\frac{\partial}{\partial x}\left(h^3\frac{\partial p^2}{\partial x}\right)+\frac{\partial}{\partial z}\left(h^3\frac{\partial p^2}{\partial z}\right)=12\,\mu R\omega\frac{\partial(ph)}{\partial x} \tag{19.6}$$

This equation can be written in nondimensional form as

$$\frac{\partial}{\partial\theta}\left(H^3\frac{\partial\overline{p}^2}{\partial\theta}\right)+\left(\frac{D}{L}\right)^2\frac{\partial}{\partial\zeta}\left(H^3\frac{\partial\overline{p}^2}{\partial\zeta}\right)=2\Lambda\frac{\partial(\overline{p}H)}{\partial\theta} \tag{19.7}$$

where

$$\overline{p}\equiv\frac{p}{p_a}\qquad p_a=\text{ambient or supply pressure}$$

$$H\equiv\frac{h}{C}\qquad\zeta=\frac{z}{L/2}\qquad\Lambda\equiv\frac{6\mu\omega}{p_a}\left(\frac{R}{C}\right)^2$$

Here Λ is called the *bearing,* or *compressibility, number.*

To solve the Reynolds equation, we require an expression for the *film thickness h.* From the triangle *ABC* in Fig. 19.5, we may write

$$\overline{AC}=h+R=R_b\cos\xi+e\cos\theta$$

where θ is measured from the line of centers. And since $e \ll R_b$, $\cos\xi \sim 1$, and thus

$$h=R_b-R+e\cos\theta$$

The *radial clearance* is $C \equiv R_b - R$, and the *eccentricity ratio* is $\varepsilon \equiv e/C$; hence

$$h=C(1+\varepsilon\cos\theta) \tag{19.8}$$

19.4.2 Boundary Conditions

Three sets of circumferential boundary conditions are commonly applied to the solutions of the Reynolds equation. These boundary conditions have been given the

names *Sommerfeld, Gumbel,* and *Swift-Stieber.* Of the three, the Sommerfeld conditions are the easiest to apply, but they yield certain unrealistic results. For example, in a liquid-lubricated bearing, Sommerfeld conditions produce negative pressures in the film. This results in the shaft's being displaced at right angles to the load line as the load is increased. Gumbel conditions are similar to Sommerfeld conditions except that all negative pressures are disregarded. Although this approach leads to more realistic load results, it produces a violation of the conservation of mass. The Swift-Stieber conditions come closest to representing the actual conditions in a film, but they are more difficult to apply. They are widely used in numerical investigations. The three sets of boundary conditions are summarized in Table 19.7.

19.5 JOURNAL BEARING PERFORMANCE

Once the pressure distribution is established, the journal bearing performance may be determined. Performance is generally measured in terms of four quantities: bearing load capacity, frictional losses, lubricant flow requirement, and temperature rise.

19.5.1 Bearing Load Relations

Five parameters are associated with the load capacity of a journal bearing:

1. The radial load component W_R acts along the line of centers (Fig. 19.1) and is computed from

$$W_R = -R \int_{-L/2}^{L/2} \int_{\theta_1}^{\theta_3} p \cos \theta \, d\theta \, dz$$

TABLE 19.7 Typical Boundary Conditions on the Reynolds Equation

Names associated with boundary conditions	Pressure profile	Mathematical expression
Sommerfeld (full Sommerfeld)	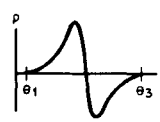	$p(\theta_1) = p(\theta_3) = 0$ (zero pressure means ambient or atmospheric pressure) For complete journal bearings: $\theta_1 = 0$, $\theta_3 = 2\pi$ For partial journal bearings: $\theta_1 = \beta_1$, $\theta_3 = \theta_1 + \beta$
Gumbel (half Sommerfeld)	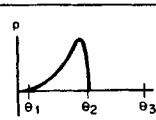	$p(\theta_1) = p(\theta_2) = 0$ $p(\theta_2 \leq \theta \leq \theta_3) = 0$ For complete journal bearings: $\theta_1 = 0$, $\theta_2 = \pi$, $\theta_3 = 2\pi$
Swift-Stieber (Reynolds)	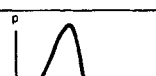	$p(\theta_2) = p_{cav}$ = atmospheric pressure $\frac{\partial p}{\partial \theta}(\theta_2) = 0$ $\theta_2 = \theta_{cav}$ which must be determined

where θ_1 and θ_3 are, respectively, the leading and trailing angular locations of the lubricating film.

2. The tangential load component W_T acts perpendicular to the line of centers:

$$W_T = R \int_{-L/2}^{L/2} \int_{\theta_1}^{\theta_3} p \sin \theta \, d\theta \, dz$$

3. The bearing load W must be supported by the pressure developed within the lubricating film. Generally the load is specified or enters the design via the *unit load P,* which is defined as the load per unit projected area, or

$$P = \frac{W}{LD}$$

Typical values of the unit load are given in Table 19.8.

TABLE 19.8 Range of Unit Loads for Various Applications

Application	Bearing	Unit load range, kpsi
Automotive engines	Main	0.6–0.8
	Crankpin	1.7–2.3
Diesel engines	Main	0.9–2.3
	Crankpin	1.1–2.3
	Wristpin	2.0–2.3
Steam turbines	Main	0.12–0.25
Air compressors	Main	0.14–0.28
	Crankpin	0.28–0.5
Centrifugal pumps	Shaft	0.1–0.18
Electric motors	Shaft	0.12–0.25

4. The *Sommerfeld number S* is a dimensionless parameter that characterizes bearing performance; large S (say, greater than 0.15) indicates a lightly loaded bearing operating at a small eccentricity. The Sommerfeld number may be calculated from

$$S = \frac{\mu UL}{\pi W} \left(\frac{R}{C}\right)^2 = \frac{\mu N}{P} \left(\frac{R}{C}\right)^2$$

5. The *attitude angle* ϕ is the angular distance between the load line and the line of centers (Fig. 19.1). It locates the minimum film thickness as measured from the load line. Because $W_R = W \cos \phi$ and $W_T = W \sin \phi$,

$$\phi = \tan^{-1} \frac{W_T}{W_R}$$

19.5.2 Bearing Friction Relations

Four parameters are involved with the frictional behavior of a journal bearing:

1. The *shear stress* τ, acting on either the shaft or the bearing surface, consists of two terms; one is due to motion of the shaft (pure shear), and the other is due to the circumferential pressure distribution (pressure-induced shear):

$$\tau = \frac{\mu U}{h} \pm \frac{h}{2R}\frac{\partial p}{\partial \theta}$$

   The plus sign corresponds to the shear stress on the journal surface; the minus sign, to the shear stress on the bearing surface.

2. The *frictional force* acting on the journal F_j is found by integrating the pure shear stress over the entire surface of the journal and the pressure-induced shear stress up to the trailing edge of the film. This yields

$$F_j = \left(\frac{2\pi}{1-\varepsilon^2}\right)(\mu UL)\left(\frac{R}{C}\right) + \frac{\varepsilon W_T}{2}\left(\frac{C}{R}\right)$$

3. The *friction coefficient* f is the ratio of the journal frictional force to the bearing load:

$$f = \frac{F_j}{W}$$

   The *friction variable* is the product $(R/C)(f)$ and so may be written

$$\left(\frac{R}{C}\right)(f) = \left(\frac{2\pi^2}{1-\varepsilon^2}\right)(S) + \frac{\varepsilon \sin \phi}{2}$$

4. The power that must be supplied to the journal to overcome friction is called the *frictional horsepower loss* HP, and it may be computed from

$$\text{HP} = C_1 F_j U = C_2 f W R N$$

   where C_1 and C_2 depend on the system of units. For F_j in pounds (lb) and U in inches per second (in/s), $C_1 = 1/6600$ for W (lb), R (in), and N in revolutions per second (r/s), $C_2 = 2\pi C_1 = 9.51998 \times 10^{-4}$.

The relevant geometry for the execution of these tasks is depicted in Fig. 19.5.

19.5.3 Lubricant Flow Relations

Lubricant flow rates are needed to estimate the capacity of the lubricant supply system and to determine the cooling requirements of the bearing. This involves evaluation of the lubricant flow within the clearance space, the lubricant flow that leaks out the sides of the bearing, and the lubricant flow that is supplied to the bearing.

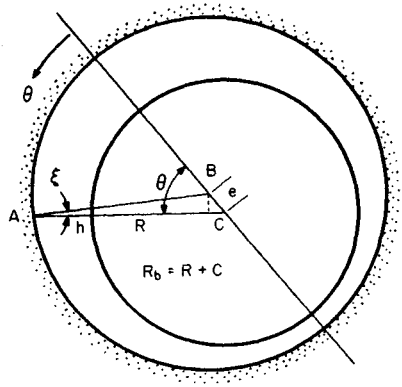

FIGURE 19.5 Film thickness geometry

In general, volume flow rate per unit length is composed of a term due to surface motion (shear flow) and another due to the pressure (pressure-induced flow). Journal bearing circumferential and axial flows per unit length are

$$q_\theta = \frac{Uh}{2} - \frac{h^3}{12\mu R}\frac{\partial p}{\partial \theta} \qquad q_z = -\frac{h^3}{12\mu}\frac{\partial p}{\partial z} \tag{19.9}$$

The total flow rates may be found by integrating Eq. (19.9) across the bearing length for the circumferential flow rate and around the bearing circumference for the axial flow rate.

Assuming that lubricant is supplied in the unloaded portion of the bearing (Fig.19.6), we see that the rate at which lubricant leaks out of the active portion of the film is

$$Q_{sa} = Q_1 - Q_2 \tag{19.10}$$

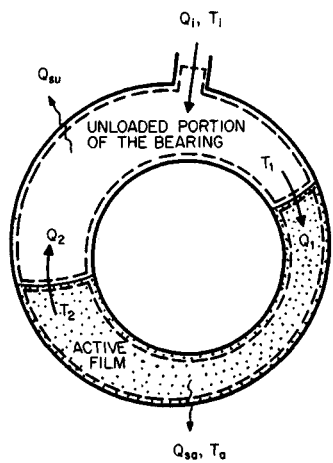

FIGURE 19.6 Control volumes for lubricant flow and heat balances.

where Q_1 = flow into the leading edge of the film and Q_2 = flow out of the trailing edge.

When the input flow rate equals the leakage flow rate, Q_1 is called the *classical rate.* For given values of *W, U,* and μ, the classical rate is the largest flow that can be carried into the active film by shaft rotation. However, in practice, Q_i, the input flow rate, may be greater (the *flooded condition*) or less (the *starved condition*) than the appropriate value to achieve the classical rate. For flooded conditions, side flow will also occur in the unloaded portion of the bearing, and we may write

$$Q_{su} = Q_2 + Q_i - Q_1 \tag{19.11}$$

Thus, $Q_{su} + Q_{sa} = Q_s = Q_i$

19.5.4 Bearing Thermal Relations

The steady energy balance equation can be simply expressed as

Energy inflow rate – energy outflow rate + energy generation rate = 0

An energy balance may be performed on the unloaded portion of the film (Fig. 19.6). Toward that end, it is assumed that there is complete mixing between the inlet

Q_i and the carryover Q_2 flows so that $T_u = T_1$. It is further assumed that there is no energy generation and negligible heat transfer. Hence, for the unloaded portion of the film,

$$Q_i T_i + Q_2 T_2 = (Q_2 + Q_i)(T_1) \tag{19.12}$$

Next an energy balance is performed on the active portion of the lubricating film (Fig. 19.6). The energy generation rate is taken to be $F_j U/J$, and the conduction heat losses to the shaft and bearing are taken to be a portion of the heat generation rate, or $\lambda F_j U/J$. Accordingly,

$$\rho Q_1 C^* T_1 - (\rho Q_{sa} C^* T_a + \rho Q_2 C^* T_2) + \frac{(1-\lambda) F_j U}{J} = 0 \tag{19.13}$$

Combining Eqs. (19.10) to (19.13) and assuming that the side-flow leakage occurs at the average film temperature $T_a = (T_1 + 2\,T_2)/2$, we find that

$$\frac{J\rho C^*(T_a - T_i)}{(1-\lambda)P} = \frac{1 + 2Q_2/Q_i}{2 - Q_{sa}/Q_1} \frac{4\pi(R/C)(f)}{Q_1/(RCNL)} \tag{19.14}$$

This shows that the lubricant temperature rise is $1 - \lambda$ times the rise when conduction is neglected.

19.6 LIQUID-LUBRICATED JOURNAL BEARINGS

In the hydrodynamic operation of a liquid-lubricated journal bearing, it is generally assumed that the lubricant behaves as a continuous incompressible fluid. However, unless the lubricant is admitted to the bearing under relatively high hydrostatic head, the liquid film can experience periodic vaporization which can cause the film to rupture and form unstable pockets, or cavities, within the film. This disruption of the film is called *cavitation,* and it occurs when the pressure within the bearing falls to the vapor pressure of the lubricant. Narrow liquid-lubricated bearings are especially susceptible to this problem. Figure 19.7 illustrates the general film condition in which lubricant is admitted through a lubricating groove at some angular position θ_0. Clearly incomplete films complicate the analysis, and therefore the design, of a liquid-lubricated journal bearing.

19.6.1 *L/D* Effects on Cylindrical Full Journal Bearings

Long-Length Bearings. When the length of a bearing is such that $L > 2D$, the axial pressure flow term in the Reynolds equation may be neglected and the bearing performs as if it were infinitely long. Under this condition, the reduced Reynolds equation can be directly integrated. Table 19.9 contains long-bearing results for both Sommerfeld and Gumbel boundary conditions.

Short-Length Bearings. When the length of a bearing is such that $L < D/4$, the axial pressure flow will dominate over the circumferential flow, and again the Reynolds equation can be readily integrated. Results of such a short-bearing integration with Gumbel boundary conditions are shown in Table 19.10.

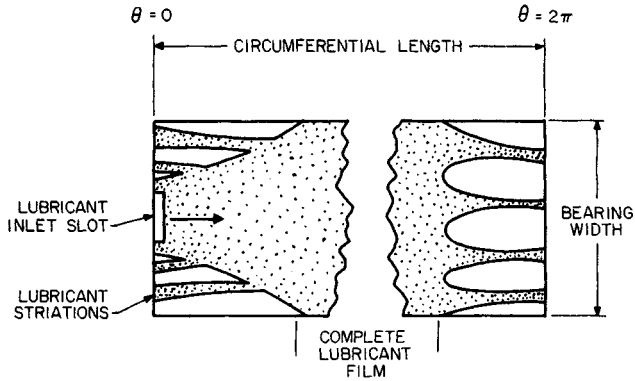

FIGURE 19.7 Diagram of an incomplete fluid film.

TABLE 19.9 Long-Bearing Pressure and Performance Parameters

Performance parameter	Sommerfeld conditions	Gumbel conditions
$\frac{p}{12\pi\mu N}\left(\frac{C}{R}\right)^2$	$\frac{(\varepsilon \sin\theta)(2+\varepsilon\cos\theta)}{(2+\varepsilon^2)(1+\varepsilon\cos\theta)^2}$	$\frac{(\varepsilon \sin\theta)(2+\varepsilon\cos\theta)}{(2+\varepsilon^2)(1+\varepsilon\cos\theta)^2}$ $0<\theta\ \pi$, $0, \pi<\theta<2\pi$
$\frac{W_R}{3\mu UL}\left(\frac{C}{R}\right)^2$	0	$\frac{4\varepsilon^2}{(2+\varepsilon^2)(1-\varepsilon^2)}$
$\frac{W_T}{3\mu UL}\left(\frac{C}{R}\right)^2$	$\frac{4\pi\varepsilon}{(2+\varepsilon^2)\sqrt{1-\varepsilon^2}}$	$\frac{2\pi\varepsilon}{(2+\varepsilon^2)\sqrt{1-\varepsilon^2}}$
ϕ	$\frac{\pi}{2}$	$\tan^{-1}\left(\frac{\pi}{2}\frac{\sqrt{1-\varepsilon^2}}{\varepsilon}\right)$
S	$\frac{(2+\varepsilon^2)\sqrt{1-\varepsilon^2}}{12\pi^2\varepsilon}$	$\frac{(2+\varepsilon^2)(1-\varepsilon^2)}{6\pi\varepsilon\sqrt{4\varepsilon^2+\pi^2(1-\varepsilon^2)}}$
$\frac{F_j}{\mu UL}\frac{C}{R}$	$\frac{4\pi(1+2\varepsilon^2)}{(2+\varepsilon^2)\sqrt{1-\varepsilon^2}}$	$\frac{\pi(4+5\varepsilon^2)}{(2+\varepsilon^2)\sqrt{1-\varepsilon^2}}$
$\left(\frac{R}{C}\right)(f)$	$\frac{1+2\varepsilon^2}{3\varepsilon}$	$\frac{4+5\varepsilon^2}{6\varepsilon}\sqrt{\frac{1-\varepsilon^2}{4\varepsilon^2+\pi(1-\varepsilon^2)}}$
$\frac{Q_s}{RCNL}$	0	0

TABLE 19.10 Short-Bearing Pressure and Performance Parameters

Performance parameter	Gumbel conditions
$\frac{p}{12\pi\mu N}\left(\frac{C}{R}\right)^2$	$-\frac{\varepsilon \sin\theta}{2(1+\varepsilon\cos\theta)^3}\left(\frac{L}{D}\right)^2(\zeta^2-1)$ $0 \le \theta \le \pi$, $0, \pi \le \theta \le 2\pi$
$\frac{W_R}{3\mu UL}\left(\frac{C}{R}\right)^2$	$\frac{4\varepsilon^2}{3(1-\varepsilon^2)^2}\left(\frac{L}{D}\right)^2$
$\frac{W_T}{3\mu UL}\left(\frac{C}{R}\right)^2$	$\frac{\pi\varepsilon^2}{3(1-\varepsilon^2)^3}\left(\frac{L}{D}\right)^2$
$\frac{W}{3\mu UL}\left(\frac{C}{R}\right)^2$	$\frac{\varepsilon\sqrt{\pi^2(1-\varepsilon^2)+16\varepsilon^2}}{3(1-\varepsilon^2)^2}\left(\frac{L}{D}\right)^2$
ϕ	$\tan^{-1}\frac{\pi(1-\varepsilon^2)^2}{4\varepsilon}$
S	$\frac{(1-\varepsilon^2)^2}{\pi\varepsilon\sqrt{\pi^2(1-\varepsilon^2)+16\varepsilon^2}}\left(\frac{D}{L}\right)^2$
$\frac{F_j}{\mu UL}\frac{C}{R}$	$\frac{2\pi}{\sqrt{1-\varepsilon^2}}$
$\left(\frac{R}{C}\right)(f)$	$\frac{(2\pi)(1-\varepsilon^2)^{3/2}}{\varepsilon\sqrt{\pi^2(1-\varepsilon^2)+16\varepsilon^2}}$
$\frac{Q_s}{RCNL}$	$2\pi\varepsilon$

Finite-Length Bearings. The *slenderness ratio L/D* for most practical designs ranges between 0.5 and 2.0. Thus, neither the short-bearing theory nor the long-bearing theory is appropriate. Numerous attempts have been made to develop methods which simultaneously account for both length and circumferential effects. Various analytical and numerical methods have been successfully employed. Although such techniques have produced important journal bearing design information, other simplified methods of analysis have been sought. These methods are useful because they do not require specialized analytical knowledge or the availability of large computing facilities. What is more, some of these simple, approximate methods yield results that have been found to be in good agreement with the more exact results. One method is described.

Reason and Narang [19.5] have developed an approximate technique that makes use of both long- and short-bearing theories. The method can be used to accurately design steadily loaded journal bearings on a hand-held calculator.

It was proposed that the film pressure p be written as a harmonic average of the short-bearing pressure p_0 and the long-bearing pressure p_∞, or

$$\frac{1}{p} = \frac{1}{p_0} + \frac{1}{p_\infty} \quad \text{or} \quad p = \frac{p_0}{1 + p_0/p_\infty}$$

The pressure and various performance parameters that can be obtained by this combined solution approximation are presented in Table 19.11. Note that several of these parameters are written in terms of two quantities, I_s and I_c. Accurate values of these quantities and the Sommerfeld number are displayed in Table 19.12. With the exception of the entrainment flow, which is increasingly overestimated at large ε and L/D, the predictions of this simple method have been found to be very good.

Example 1. Using the Reason and Narang combined solution approximation, determine the performance of a steadily loaded full journal bearing for the following conditions:

$\mu = 4 \times 10^{-6}$ reyn $\quad D = 1.5$ in

$N = 1800$ r/min $\quad L = 1.5$ in

$W = 500$ lbf $\quad C = 1.5 \times 10^{-3}$

Solution. The unit load is $P = W/(LD) = 222$ pounds per square inch (psi), and the Sommerfeld number is

$$S = \frac{\mu N}{P}\left(\frac{R}{C}\right)^2 = 0.135$$

Entering Table 19.12 at this Sommerfeld number and a slenderness ratio of 1, we find that $\varepsilon = 0.582$, $I_c = 0.2391$, and $I_s = 0.3119$. The bearing performance is computed by evaluating various parameters in Table 19.11. Results are compared in Table 19.13 to values obtained by Shigley and Mischke [19.6] by using design charts.

19.6.2 Design Charts

Design charts have been widely used for convenient presentation of bearing performance data. Separate design graphs are required for every bearing configuration or variation. Use of the charts invariably requires repeated interpolations and extrapolations. Thus, design of journal bearings from these charts is somewhat tedious.

Raimondi-Boyd Charts. The most famous set of design charts was constructed by Raimondi and Boyd [19.7]. They presented 45 charts and 6 tables of numerical information for the design of bearings with slenderness ratios of ¼, ½, and 1 for both partial (60°, 120°, and 180°) and full journal bearings. Consequently, space does not permit all those charts to be presented. Instead a sampling of the charts for bearings with an L/D ratio of 1 is given. Figures 19.8 to 19.13 present graphs of the *minimum-film-thickness variable* h_0/C (note that $h_0/C = 1 - \varepsilon$), the *attitude angle* ϕ (or location of the minimum thickness), the *friction variable* $(R/C)(f)$, the *flow variable* $Q/(RCNL)$, the *flow ratio* Q_s/Q, and the *temperature-rise variable* $J\rho C^* \Delta T/P$. Table 19.14 is a tabular presentation of these data.

TABLE 19.11 Pressure and Performance Parameters of the Combined Solution Approximation

Performance parameter	Equation
$\frac{p}{12\pi\mu N}\left(\frac{C}{R}\right)^2$	$\dfrac{\frac{1}{2}\left(\frac{L}{D}\right)^2(1-\zeta^2)\dfrac{\varepsilon\sin\theta}{(1+\varepsilon\cos\theta)^3}}{1+\left(\frac{L}{D}\right)^2\dfrac{(2+\varepsilon^2)(1-\zeta^2)}{2(1+\varepsilon\cos\theta)(2+\varepsilon\cos\theta)}}$
$\frac{W_R}{3\mu UL}\left(\frac{C}{R}\right)^2$	$-2I_c$
$\frac{W_T}{3\mu UL}\left(\frac{C}{R}\right)^2$	$2I_s$
ϕ	$\tan^{-1}\left(\frac{-I_s}{I_c}\right)$
S	$\dfrac{1}{6\pi\sqrt{I_s^2+I_c^2}}$
$\frac{F_j}{\mu UL}\frac{C}{R}$	$3\varepsilon I_s+\dfrac{2\pi}{\sqrt{1-\varepsilon^2}}$
$\left(\frac{R}{C}\right)(f)$	$6\pi S\left(\frac{\varepsilon I_S}{2}+\dfrac{\pi}{3\sqrt{1-\varepsilon^2}}\right)$
$\frac{Q_{0,\pi}}{RCNL}$ †	$\pi\left[1+\varepsilon\mp\varepsilon E\left(1-\dfrac{2E}{\sqrt{1+2E}}\tanh^{-1}\dfrac{1}{\sqrt{1+2E}}\right)\left(\frac{L}{D}\right)^2\right]$ where $E=\dfrac{(1\pm\varepsilon)(2\pm\varepsilon)}{(2+\varepsilon^2)}\left(\frac{D}{L}\right)^2$
$\frac{Q_s}{Q_0}$	$1-\dfrac{Q_\pi}{Q_0}$
$\frac{J\rho C^*\Delta T}{P}$	$\dfrac{1}{1-\frac{1}{2}Q_s/Q_0}\dfrac{4\pi(R/C)f}{Q_0/(RCNL)}$

†For Q_0 (flow through maximum film thickness at $\theta = 0$) use top signs; for Q_π (flow through minimum film thickness at $\theta = \pi$) use lower signs.

TABLE 19.12 Values of I_s, I_c, and Sommerfeld Number for Various Values of L/D and ε

ε \ L/D	0.25	0.5	0.75	1.0	1.5	2	∞
0.1	0.0032†	0.0120	0.0244	0:0380	0.0636	0.0839	0.1570
	−0.0004	−0.0014	−0.0028	−0.0041	−0.0063	−0.0076	−0.0100
	16.4506	4.3912	2.1601	1.3880	0.8301	0.6297	0.3372
0.2	0.0067	0.0251	0.0505	0.0783	0.1300	0.1705	0.3143
	−0.0017	−0.0062	−0.0118	−0.0174	−0.0259	−0.0312	−0.0408
	7.6750	2.0519	1.0230	0.6614	0.4002	0.3061	0.1674
0.3	0.0109	0.0404	0.0804	0.1236	0.2023	0.2628	0.4727
	−0.0043	−0.0153	−0.0289	−0.0419	−0.0615	−0.0733	−0.0946
	4.5276	1.2280	0.6209	0.4065	0.2509	0.1944	0.1100
0.4	0.0164	0.0597	0.1172	0.1776	0.2847	0.3649	0.6347
	−0.0089	−0.0312	−0.0579	−0.0825	−0.1183	−0.1391	−0.1763
	2.8432	0.7876	0.4058	0.2709	0.1721	0.1359	0.0805
0.5	0.0241	0.0862	0.1656	0.2462	0.3835	0.4831	0.8061
	−0.0174	−0.0591	−0.1065	−0.1484	−0.2065	−0.2391	−0.2962
	1.7848	0.5076	0.2694	0.1845	0.1218	0.0984	0.0618
0.6	0.0363	0.1259	0.2345	0.3306	0.5102	0.6291	0.9983
	−0.0338	−0.1105	−0.1917	−0.2590	−0.3474	−0.3949	−0.4766
	1.0696	0.3167	0.1752	0.1242	0.0859	0.0714	0.0480
0.7	0.0582	0.1927	0.3430	0.4793	0.6878	0.8266	1.2366
	−0.0703	−0.2161	−0.3549	−0.4612	−0.5916	−0.6586	−0.7717
	0.5813	0.1832	0.1075	0.0798	0.0585	0.0502	0.0364
0.8	0.1071	0.3264	0.5425	0.7220	0.9771	1.1380	1.5866
	−0.1732	−0.4797	−0.7283	−0.8987	−0.0941	−1.1891	−0.3467
	0.2605	0.0914	0.0584	0.0460	0.0362	0.0322	0.0255
0.9	0.2761	0.7079	1.0499	1.3002	1.6235	1.8137	2.3083
	−0.6644	−1.4990	−2.0172	−2.3269	−2.6461	−2.7932	−3.0339
	0.0737	0.0320	0.0233	0.0199	0.0171	0.0159	0.0139
0.95	0.6429	1.3712	1.8467	2.1632	2.5455	2.7600	3.2913
	−2.1625	−3.9787	−4.8773	−5.3621	−5.8315	−6.0396	−6.3776
	0.0235	0.0126	0.0102	0.0092	0.0083	0.0080	0.0074
0.99	3.3140	4.9224	5.6905	6.1373	6.6295	6.8881	8.7210
	−22.0703	−28.5960	−30.8608	−31.9219	−32.8642	−33.2602	−33.5520
	0.0024	0.0018	0.0017	0.0016	0.0016	0.0016	0.0015

†The three numbers associated with each ε and L/D pair are, in order from top to bottom, I_s, I_c, and S.

TABLE 19.13 Comparison of Predicted Performance between Two Methods for Example 1

Method \ Parameter	ε	ϕ	$\left(\frac{R}{C}\right)(f)$	$\frac{Q}{RCNL}$	$\frac{Q_s}{Q}$	ΔT
Combined solution approximation	0.582	52.5°	3.508	4.473	0.652	26.6°F
Design charts†	0.58	53.°	3.50	4.28	0.655	26.6°F

†SOURCE: Shigley and Mischke [19.6].

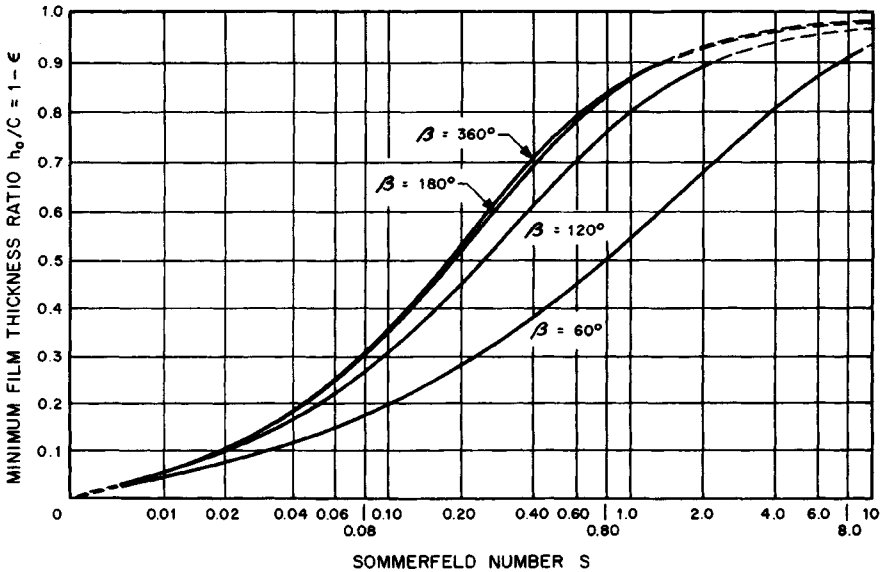

FIGURE 19.8 Minimum film thickness ratio versus Sommerfeld number for full and partial journal bearings, $L/D = 1$, Swift-Stieber boundary conditions. *(From Raimondi and Boyd [19.7].)*

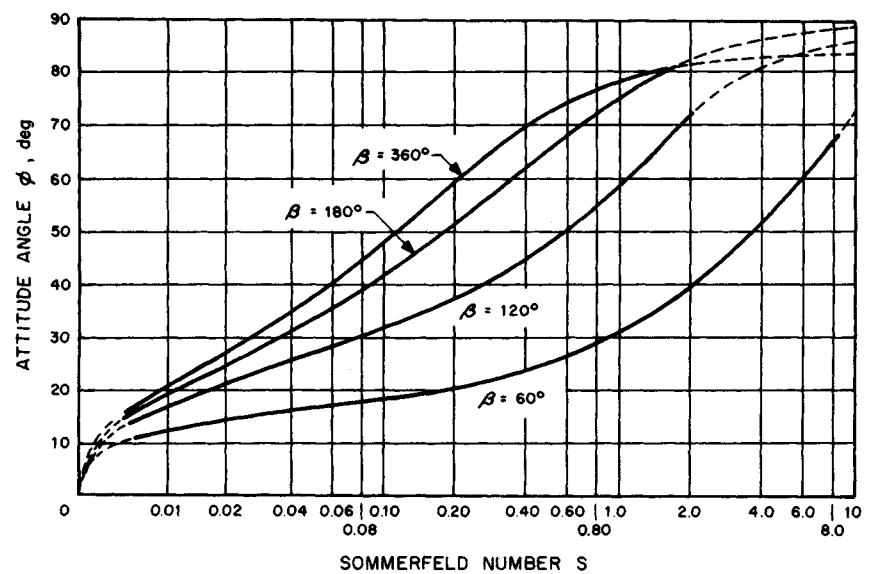

FIGURE 19.9 Attitude angle versus Sommerfeld number for full and partial journal bearings, $L/D = 1$, Swift-Stieber boundary conditions. *(From Raimondi and Boyd [19.7].)*

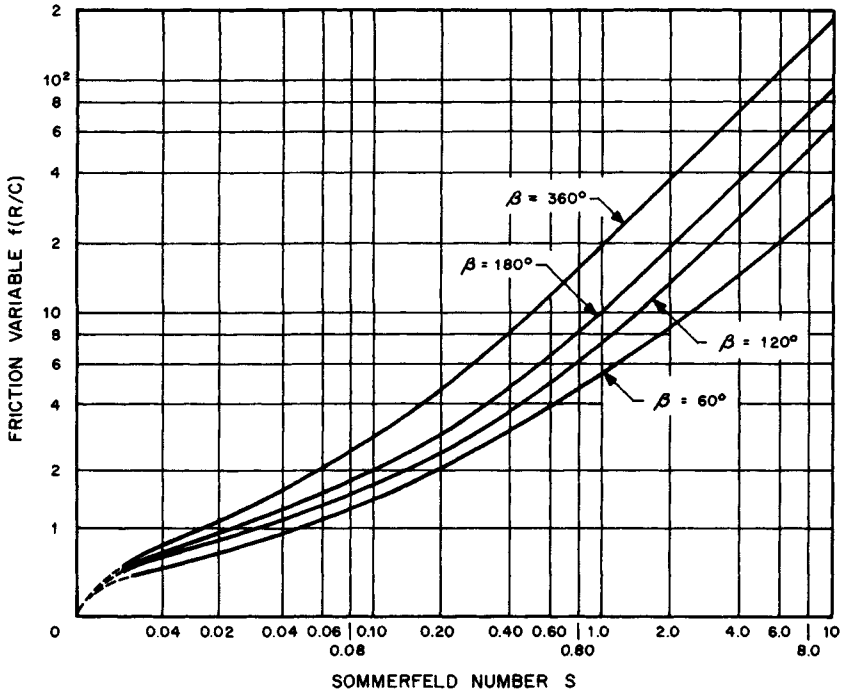

FIGURE 19.10 Friction variable versus Sommerfeld number for full and partial journal bearings, $L/D = 1$, Swift-Stieber boundary conditions. *(From Raimondi and Boyd [19.7].)*

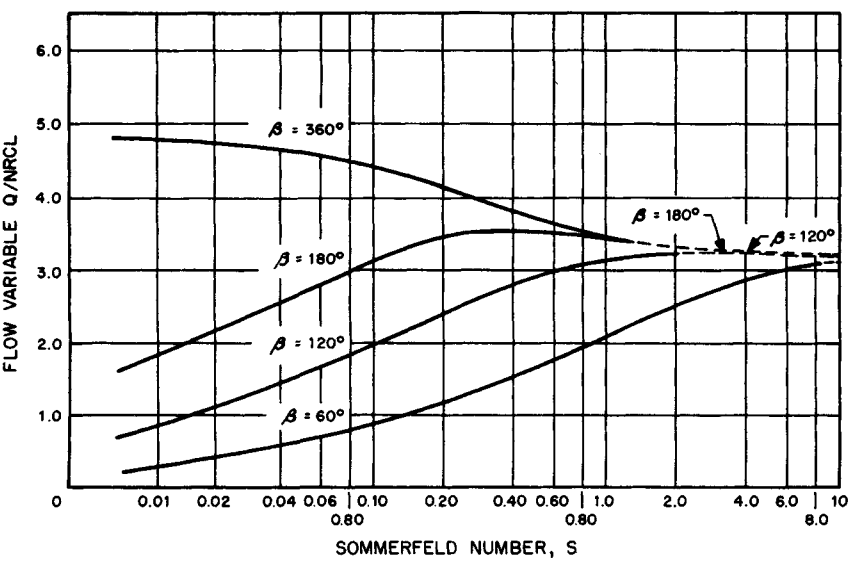

FIGURE 19.11 Flow variable versus Sommerfeld number for full and partial journal bearings, $L/D = 1$, Swift-Stieber boundary conditions. *(From Raimondi and Boyd [19.7].)*

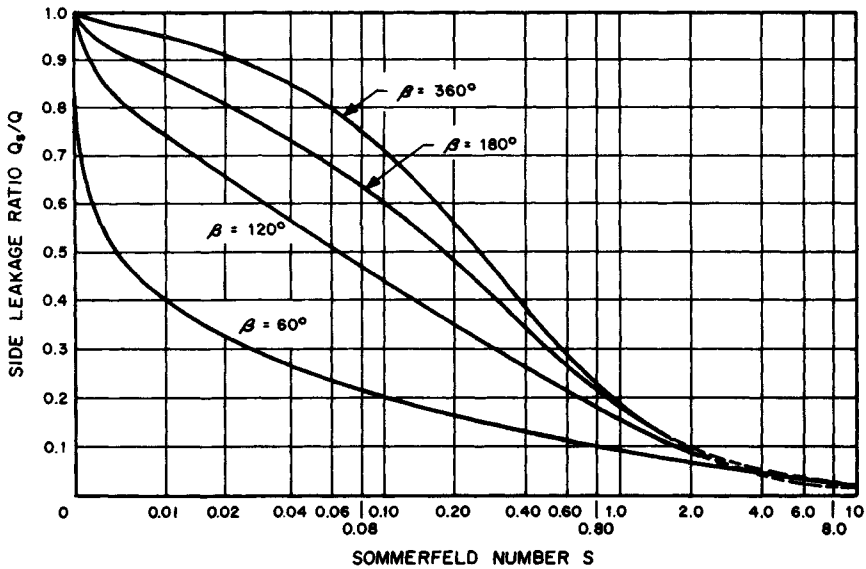

FIGURE 19.12 Side-leakage ratio versus Sommerfeld number for full and partial journal bearings, $L/D = 1$, Swift-Stieber boundary conditions. *(From Raimondi and Boyd [19.7].)*

For slenderness ratios other than the four displayed (∞, 1, ½, and ¼), Raimondi and Boyd suggest the use of the following interpolation formula:

$$y_{L/D} = \left(\frac{D}{L}\right)^3 \left[-\frac{1}{8}\left(1-\frac{L}{D}\right)\left(1-2\frac{L}{D}\right)\left(1-4\frac{L}{D}\right)y_\infty + \frac{1}{3}\left(1-2\frac{L}{D}\right)\left(1-4\frac{L}{D}\right)y_1 - \frac{1}{4}\left(1-\frac{L}{D}\right)\left(1-4\frac{L}{D}\right)y_{1/2} + \frac{1}{24}\left(1-\frac{L}{D}\right)\left(1-2\frac{L}{D}\right)y_{1/4}\right]$$

where y = any performance variable, that is, $(R/C)(f)$, h_0/C, etc., and the subscript of y is the L/D value at which the variable is being evaluated.

For partial bearings with bearing arc angles other than the three displayed (180°, 120°, and 60°), Raimondi and Boyd recommend using the following interpolation formula:

$$y_\beta = \frac{1}{7200}\left[(\beta-120)(\beta-60)y_{180} - 2(\beta-180)(\beta-60)y_{120} + (\beta-180)(\beta-120)y_{60}\right]$$

where y = any performance variable and the subscript of y is the β at which the variable is being evaluated.

Some of the tedium associated with use of charts can be removed by employing curve fits of the data. Seireg and Dandage [19.8] have developed approximate equations for the full journal bearing data of the Raimondi and Boyd charts. Table 19.15 gives the coefficients to be used in these curve-fitted equations.

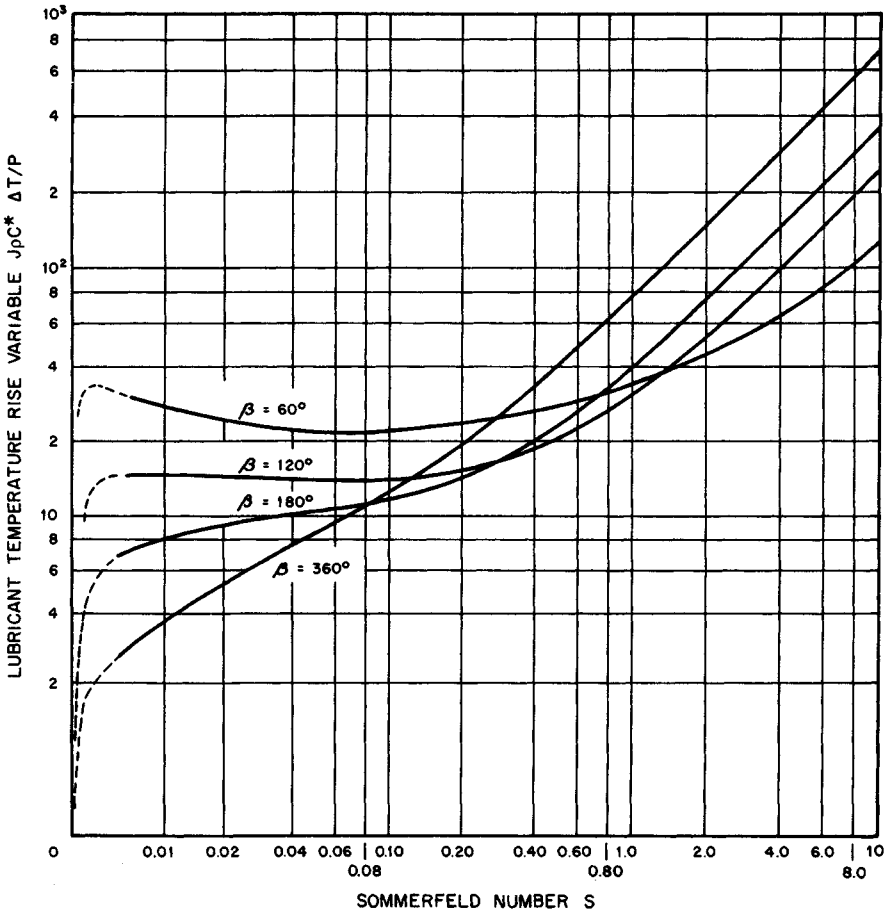

FIGURE 19.13 Lubricant temperature-rise variable versus Sommerfeld number for full and partial journal bearings, $L/D = 1$, Swift-Stieber boundary conditions. *(From Raimondi and Boyd [19.7].)*

Example 2. For the following data

$N = 3600$ r/min	$L = 4$ in
$W = 7200$ lbf	$C = 6.0 \times 10^{3}$ in
$D = 6$ in	Lubricant: SAE 20 oil
	Inlet temperature $T_i = 110°F$

determine the isoviscous performance of a centrally loaded full journal bearing. The viscosity-temperature relation is contained in Table 19.16.

Solution. Because the viscosity varies with temperature, an iterative procedure is required. By this procedure, a first-guess viscosity is used to determine the film temperature rise. From this an average film temperature is determined, which will permit a second film temperature rise to be determined, and so on, until a converged result is obtained.

TABLE 19.14 Performance Data for Full and Partial Journal Bearings, $L/D = 1$, Swift-Stieber Boundary Conditions

L/D	ε	θ_1	S	ϕ	$\left(\frac{R}{C}\right)(f)$	$\frac{Q}{RCNL}$	$\frac{Q_s}{Q}$	$\frac{JpC^* \Delta T}{P}$
				Full bearing				
∞	0.1	0	0.240	69.10	4.80	3.03	0	19.9
	0.2	0	0.123	67.26	2.57	2.83	0	11.4
	0.4	0	0.0626	61.94	1.52	2.26	0	8.47
	0.6	0	0.0389	54.31	1.20	1.56	0	9.73
	0.8	0	0.0210	42.22	0.961	0.760	0	15.9
	0.9	0	0.0115	31.62	0.756	0.411	0	
1	0.1	0	1.33	79.5	26.4	3.37	0.150	106
	0.2	0	0.631	74.02	12.8	3.59	0.280	52.1
	0.4	0	0.264	63.10	5.79	3.99	0.497	24.3
	0.6	0	0.121	50.58	3.22	4.33	0.680	14.2
	0.8	0	0.0446	36.24	1.70	4.62	0.842	8.00
	0.9	0	0.0188	26.45	1.05	4.74	0.919	5.16
	0.97	0	0.00474	15.47	0.514	4.82	0.973	2.61
1/2	0.1	0	4.31	81.62	85.6	3.43	0.173	343
	0.2	0	2.03	74.94	40.9	3.72	0.318	164
	0.4	0	0.779	61.45	17.0	4.29	0.552	68.6
	0.6	0	0.319	48.14	8.10	4.85	0.730	33.0
	0.8	0	0.0923	33.31	3.26	5.41	0.874	13.4
	0.9	0	0.0313	23.66	1.60	5.69	0.939	6.66
	0.97	0	0.00609	13.75	0.610	5.88	0.980	2.56
1/4	0.1	0	16.2	82.31	322	3.45	0.180	1287
	0.2	0	7.57	75.18	153	3.76	0.330	611
	0.4	0	2.83	60.86	61.1	4.37	0.567	245
	0.6	0	1.07	46.72	26.7	4.99	0.746	107
	0.8	0	0.261	31.04	8.80	5.60	0.884	35.4
	0.9	0	0.0736	21.85	3.50	5.91	0.945	14.1
	0.97	0	0.0101	12.22	0.922	6.12	0.984	3.73
				Partial bearing, $\beta = 60°$				
∞	0.1	84.00	5.75	65.91	19.7	3.01	0	82.3
	0.2	101.00	2.66	48.91	10.1	2.73	0	46.5
	0.4	118.00	0.931	31.96	4.67	2.07	0	28.4
	0.6	126.80	0.322	23.21	2.40	1.40	0	21.5
	0.8	132.60	0.0755	17.39	1.10	0.722	0	19.2
	0.9	135.06	0.0241	14.94	0.667	0.372	0	22.5
	0.97	139.14	0.00495	10.88	0.372	0.115	0	40.7
1	0.1	82.00	8.52	67.92	29.1	3.07	0.0267	121
	0.2	99.00	3.92	50.96	14.8	2.82	0.0481	67.4
	0.4	116.00	1.34	33.99	6.61	2.22	0.0849	39.1
	0.6	125.50	0.450	24.56	3.29	1.56	0.127	28.2
	0.8	131.60	0.101	18.33	1.42	0.883	0.200	22.5
	0.9	134.67	0.0309	15.33	0.822	0.519	0.287	23.2
	0.97	139.10	0.00584	10.88	0.422	0.226	0.465	30.5

TABLE 19.14 Performance Data for Full and Partial Journal Bearings, $L/D = 1$, Swift-Stieber Boundary Conditions (*Continued*)

L/D	ε	θ_1	S	ϕ	$\left(\frac{R}{C}\right)(f)$	$\frac{Q}{RCNL}$	$\frac{Q_s}{Q}$	$\frac{J\rho C^* \Delta T}{P}$
				Partial bearing, $\beta = 60°$ (*Continued*)				
1/2	0.1	81.00	14.2	69.00	48.6	3.11	0.0488	201
	0.2	97.50	6.47	52.60	24.2	2.91	0.0883	109
	0.4	113.00	2.14	37.00	10.3	2.38	0.160	59.4
	0.6	123.00	0.695	26.98	4.93	1.74	0.236	40.3
	0.8	130.40	0.149	19.57	2.02	1.05	0.350	29.4
	0.9	134.09	0.0422	15.91	1.08	0.664	0.464	26.5
	0.97	139.22	0.00704	10.85	0.490	0.329	0.650	27.8
1/4	0.1	78.50	35.8	71.55	121	3.16	0.0666	499
	0.2	91.50	16.0	58.51	58.7	3.04	0.131	260
	0.4	109.00	5.20	41.01	24.5	2.57	0.236	136
	0.6	119.80	1.65	30.14	11.2	1.98	0.346	86.1
	0.8	128.30	0.333	21.70	4.27	1.30	0.496	54.9
	0.9	133.10	0.0844	16.87	2.01	0.894	0.620	41.0
	0.97	139.20	0.0110	10.81	0.713	0.507	0.786	29.1
				Partial bearing, $\beta = 120°$				
∞	0.1	53.300	0.877	66.69	6.02	3.02	0	25.1
	0.2	67.400	0.431	52.60	3.26	2.75	0	14.9
	0.4	81.000	0.181	39.02	1.78	2.13	0	10.5
	0.6	87.300	0.0845	32.67	1.21	1.47	0	10.3
	0.8	93.200	0.0328	26.80	0.853	0.759	0	14.1
	0.9	98.500	0.0147	21.51	0.653	0.388	0	21.2
	0.97	106.15	0.00406	13.86	0.399	0.118	0	42.4
1	0.1	47.500	2.14	72.43	14.5	3.20	0.0876	59.5
	0.2	62.000	1.01	58.25	7.44	3.11	0.157	32.6
	0.4	76.000	0.385	43.98	3.60	2.75	0.272	19.0
	0.6	84.500	0.162	35.65	2.16	2.24	0.384	15.0
	0.8	92.600	0.0531	27.42	1.27	1.57	0.535	13.9
	0.9	98.667	0.0208	21.29	0.855	1.11	0.657	14.4
	0.97	106.50	0.00498	13.49	0.461	0.694	0.812	14.0
1/2	0.1	45.000	5.42	74.99	36.6	3.29	0.124	149
	0.2	56.650	2.51	63.38	18.1	3.32	0.225	77.2
	0.4	72.000	0.914	48.07	8.20	3.15	0.386	40.5
	0.6	81.500	0.354	38.50	4.43	2.80	0.530	27.0
	0.8	92.000	0.0973	28.02	2.17	2.18	0.684	19.0
	0.9	99.000	0.0324	21.02	1.24	1.70	0.787	15.1
	0.97	107.00	0.00631	13.00	0.550	1.19	0.899	10.6
1/4	0.1	43.000	18.4	76.97	124	3.34	0.143	502
	0.2	54.000	8.45	65.97	60.4	3.44	0.260	254
	0.4	68.833	3.04	51.23	26.6	3.42	0.442	125
	0.6	79.600	1.12	40.42	13.5	3.20	0.599	75.8
	0.8	91.560	0.268	28.38	5.65	2.67	0.753	42.7
	0.9	99.400	0.0743	20.55	2.63	2.21	0.846	25.9
	0.97	108.00	0.0105	12.11	0.832	1.69	0.931	11.6

TABLE 19.14 Performance Data for Full and Partial Journal Bearings, $L/D = 1$, Swift-Stieber Boundary Conditions (*Continued*)

L/D	ε	θ_1	S	ϕ	$\left(\frac{R}{C}\right)(f)$	$\frac{Q}{RCNL}$	$\frac{Q_s}{Q}$	$\frac{J\rho C^* \Delta T}{P}$
				Partial bearing, $\beta = 180°$				
∞	0.1	17.000	0.347	72.90	3.55	3.04	0	14.7
	0.2	28.600	0.179	61.32	2.01	2.80	0	8.99
	0.4	40.000	0.0898	49.99	1.29	2.20	0	7.34
	0.6	46.900	0.0523	43.15	1.06	1.52	0	8.71
	0.8	56.700	0.0253	33.35	0.859	0.767	0	14.1
	0.9	64.200	0.0128	25.57	0.681	0.380	0	22.5
	0.97	74.650	0.00384	15.43	0.416	0.119	0	44.0
1	0.1	11.500	1.40	78.50	14.1	3.34	0.139	57.0
	0.2	21.000	0.670	68.93	7.15	3.46	0.252	29.7
	0.4	34.167	0.278	58.86	3.61	3.49	0.425	16.5
	0.6	45.000	0.128	44.67	2.28	3.25	0.572	12.4
	0.8	58.000	0.0463	32.33	1.39	2.63	0.721	10.4
	0.9	66.000	0.0193	24.14	0.921	2.14	0.818	9.13
	0.97	75.584	0.00483	14.57	0.483	1.60	0.915	6.96
1/2	0.1	10.000	4.38	79.97	44.0	3.41	0.167	177
	0.2	17.800	2.06	72.14	21.6	3.64	0.302	87.8
	0.4	32.000	0.794	58.01	9.96	3.93	0.506	42.7
	0.6	45.000	0.321	45.01	5.41	3.93	0.665	25.9
	0.8	59.000	0.0921	31.29	2.54	3.56	0.806	15.0
	0.9	67.200	0.0314	22.80	1.38	3.17	0.886	9.80
	0.97	76.500	0.00625	13.63	0.581	2.62	0.951	5.30
1/4	0.1	9.000	16.3	81.40	163	3.44	0.176	653
	0.2	16.300	7.60	73.70	79.4	3.71	0.320	320
	0.4	31.000	2.84	58.99	35.1	4.11	0.534	146
	0.6	45.000	1.08	44.96	17.6	4.25	0.698	79.8
	0.8	59.300	0.263	30.43	6.88	4.07	0.837	36.5
	0.9	68.900	0.0736	21.43	2.99	3.72	0.905	18.4
	0.97	77.680	0.0104	12.28	0.877	3.29	0.961	6.46

SOURCE: Raimondi and Boyd [19.7].

Since $L/D = \frac{2}{3}$, the Raimondi and Boyd charts would require interpolation. Alternatively, the Seireg-Dandage curve-fitted equations are used. The unit load may be immediately computed:

$$P = \frac{W}{LD} = \frac{7200}{(6)(4)} = 300 \text{ psi}$$

The first guess of viscosity is based on the inlet temperature:

$$\mu_1 = 1.36 \times 10^{-8} \exp \frac{1271.6}{110 + 95} = 6.72 \times 10^{-6} \text{ reyn}$$

$$S_1 = \frac{\mu_1 N}{P}\left(\frac{R}{C}\right)^2 = 0.336$$

TABLE 19.15 Seireg-Dandage Curve Fits of Raimondi-Boyd Charts: Variable $= a\left(\frac{L}{D}\right)^{b_1} S^{b_2 + b_3(L/D)}$

Variable	$S \leq 0.15$					$S > 0.15$				
		a	b_1	b_2	b_3		a	b_1	b_2	b_3
				$\frac{1}{2} \leq L/D \leq 1$						
$\frac{h_0}{C} = 1 - \varepsilon$	$S \leq 0.04$	2.7258	0.83621	0.75101	0.08113	$S \leq 1$	0.91437	0.4538	0.6119	−0.2890
	$S > 0.04$	1.7176	1.0478	0.4999	0.1868	$S > 1$	0.89574	0.3895	0.3076	−0.2537
ϕ, rad	.....	110.9067	0.60907	0.28856	0.07485	.....	74.0225	0.2395	0.3131	−0.2172
$\left(\frac{R}{C}\right)(f)$	.....	9.9533	−0.4758	0.6705	−0.1124	.....	3.5251	−0.2333	−0.1926	0.1149
$\frac{Q}{RCNL}$	.....	4.1036	−0.306242	−0.024799	−0.009982	.....	20.4422	−0.1125	0.8551	0.1014
$\frac{J\rho C^* \Delta T}{P}$	.....	42.0097	−0.4146	0.6869	−0.1600	.....	84.2989	−0.08167	0.85540	0.08787
$\frac{p}{p_{max}}$	.....	0.79567	0.59651	0.25659	0.04321	.....	0.52529	0.2486	0.2335	−0.1870

TABLE 19.15 Seireg-Dandage Curve Fits of Raimondi-Boyd Charts: Variable = $a\left(\frac{L}{D}\right)^{b_1} S^{b_2 + b_3(L/D)}$ (*Continued*)

Variable	$S \le 0.15$					$S > 0.15$				
		a	b_1	b_2	b_3		a	b_1	b_2	b_3
					$\frac{1}{4} \le L/D \le \frac{1}{2}$					
$\frac{h_0}{C} = 1 - \varepsilon$	$S \le 0.04$	9.2341	2.0673	0.4286	0.9247	$S \le 1$	1.1674	0.80824	0.48016	−0.02463
	$S > 0.04$	1.1545	0.4637	0.7851	−0.3788	$S > 1$	1.1263	0.7279	0.5117	−0.6581
ϕ, rad	.....	112.7756	0.6332	0.2592	0.1336	.....	93.6908	0.5313	0.3139	−0.2923
$\left(\frac{R}{C}\right)(f)$	.....	9.4896	−0.5446	0.7290	−0.2293	.....	17.1809	−0.3133	0.7993	0.2887
$\frac{Q}{RCNL}$	.....	4.5607	−0.153864	−0.005371	−0.48838	.....	3.4980	−0.23973	−0.11107	−0.04103
$\frac{JpC^* \Delta T}{P}$	.....	38.7604	−0.5307	0.7322	−0.2505	.....	69.4842	−0.3075	0.8003	0.2783
$\frac{p}{p_{max}}$	.....	0.78635	0.57952	0.23620	0.0840	.....	0.64927	0.5037	0.2783	−0.3534

SOURCE: Ref. [19.8].

TABLE 19.16 Constants for Use in Viscosity-Temperature Equation for Various Oils

Oil	μ_0†, reyn	b, °F
SAE 10	1.58×10^{-8}	1157.5
SAE 20	1.36×10^{-8}	1271.6
SAE 30	1.41×10^{-8}	1360.9
SAE 40	1.21×10^{-8}	1474.4
SAE 50	1.70×10^{-8}	1509.6
SAE 60	1.87×10^{-8}	1564.0

†$\mu = \mu_0 \exp [b/(T + 95)]$.
SOURCE: Ref. [19.8].

From Table 19.15, the appropriate curve-fitted equation for the temperature rise is

$$\Delta T = 84.2989 \frac{P}{J\rho C^*} \left(\frac{L}{D}\right)^{-0.08167} S^{0.8554 + 0.08787 L/D}$$

Taking $\rho = 0.03$ pound mass per cubic inch (lbm/in^3) and $C^* = 0.40$ Btu/(lbm · °F) as representative values for lubricating oil, we obtain

$$\Delta T_1 = 233.33(0.336)^{0.914} = 86.1°\text{F}$$

And so the second estimate of the film mean temperature is

$$T_{a2} = 110 + \frac{86.1}{2} = 153.1°\text{F}$$

Repeated calculations (13 iterations) produce

$$S = 0.176 \qquad \mu = 3.5 \times 10^{-6} \text{ reyn} \qquad \Delta T = 47.7°\text{F}$$

With the Sommerfeld number, the remaining performance parameters are easily calculated.

Connors' Lubricant Supply Charts. The Raimondi-Boyd lubricant flow and temperature rise data are based on the notion that there is no carryover flow into the active film; that is, $Q_2 = 0$ in Eq. (19.14). From an analogous view, these results are applicable to the situation where $Q_i >> Q_2$. Accordingly, Raimondi-Boyd predictions represent fully flooded bearing conditions and yield the coolest running lubricant temperatures for a given set of operating conditions, not accounting for any heat conduction losses.

To remedy this and thus provide more realistic design information, Connors [19.9] developed design charts which incorporate the influence of lubricant supply rate on the performance of a full journal bearing for $L/D = 1$. Figures 19.14 to 19.16 are plots that can be used over the entire range of flows to determine minimum film thickness, friction, and temperature rise from given values of the Sommerfeld number and the inlet flow variable.

Example 3. Determine the lubricant temperature rise as a function of the inlet flow rate for the following design parameters:

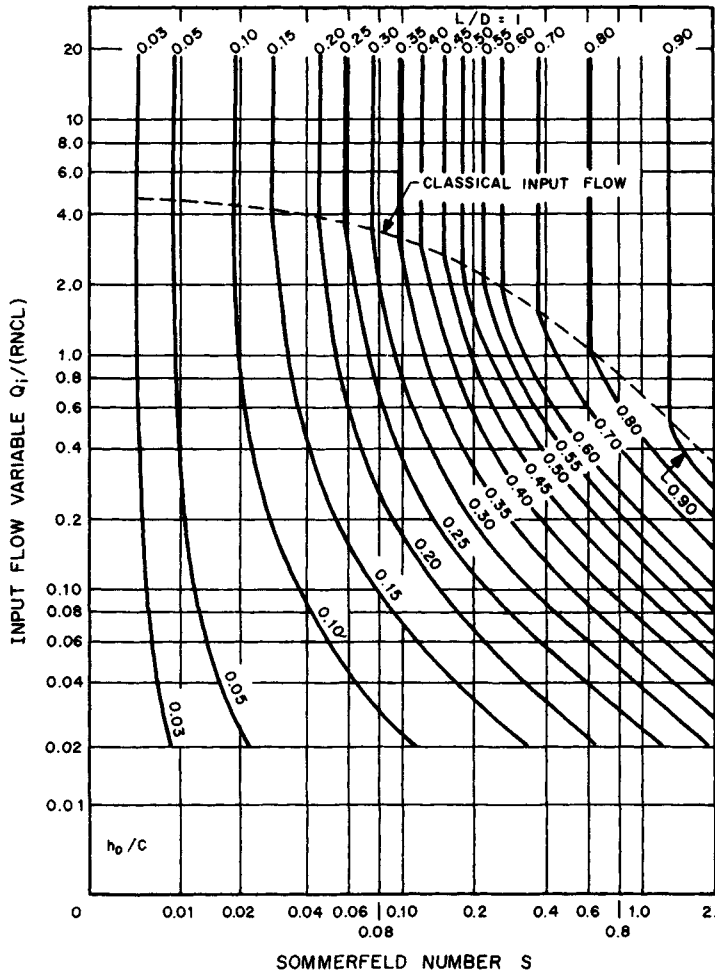

FIGURE 19.14 Inlet flow variable versus Sommerfeld number for parametric values of minimum film thickness ratio; $L/D = 1$, full journal bearing. *(From Connors [19.9].)*

$W = 1500$ lbf $\quad C = 4 \times 10^{-3}$ in

$N = 1800$ r/min $\quad$ SAE 30 oil

$D = 4$ in $\quad T_i = 100°F$

$L = 4$ in

Solution. To solve this type of problem, a plot or equation of lubricant viscosity as a function of temperature must be available. The calculation procedure is as follows:

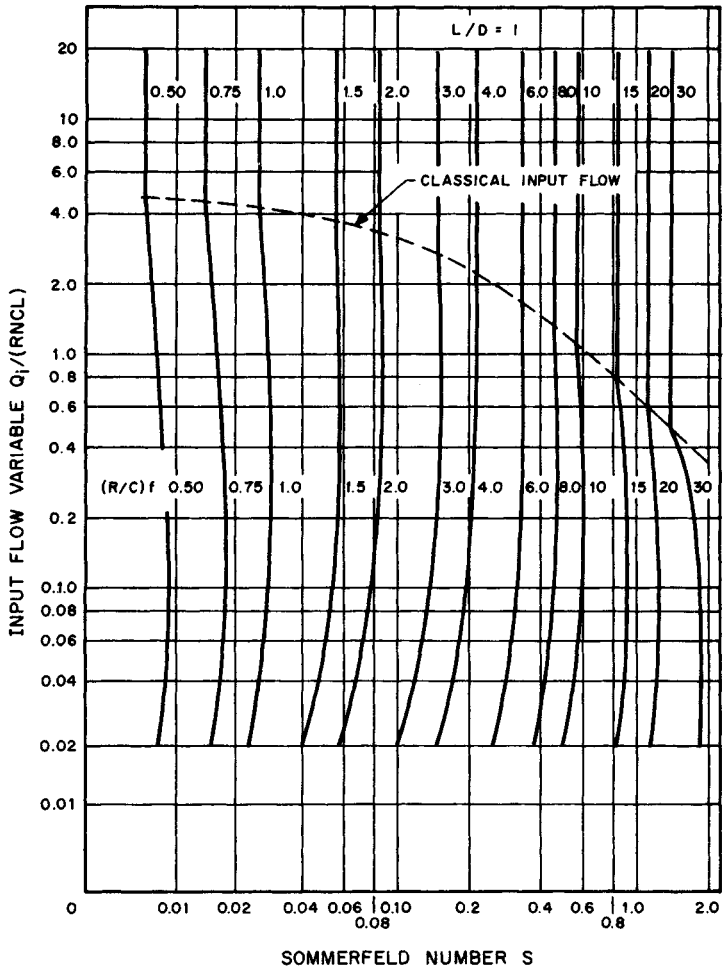

FIGURE 19.15 Inlet flow variable versus Sommerfeld number for parametric values of friction variable; $L/D = 1$, full journal bearing. *(From Connors [19.9].)*

1. Select a value of $Q_i/(RCNL)$.
2. Assume a viscosity value.
3. Compute the Sommerfeld number.
4. Use the $Q_i/(RCNL)$ and S values to find $J\rho C^*(T_a - T_i)/P$ in Fig. 19.16.
5. Calculate the mean film temperature T_a.
6. Increment μ and repeat the process from step 3 until there are sufficient points to establish an intersection with the lubricant's μ versus T data. This intersection represents the operating point for the given $Q_i/(RNCL)$.
7. Increment the input flow variable, and return to step 2.

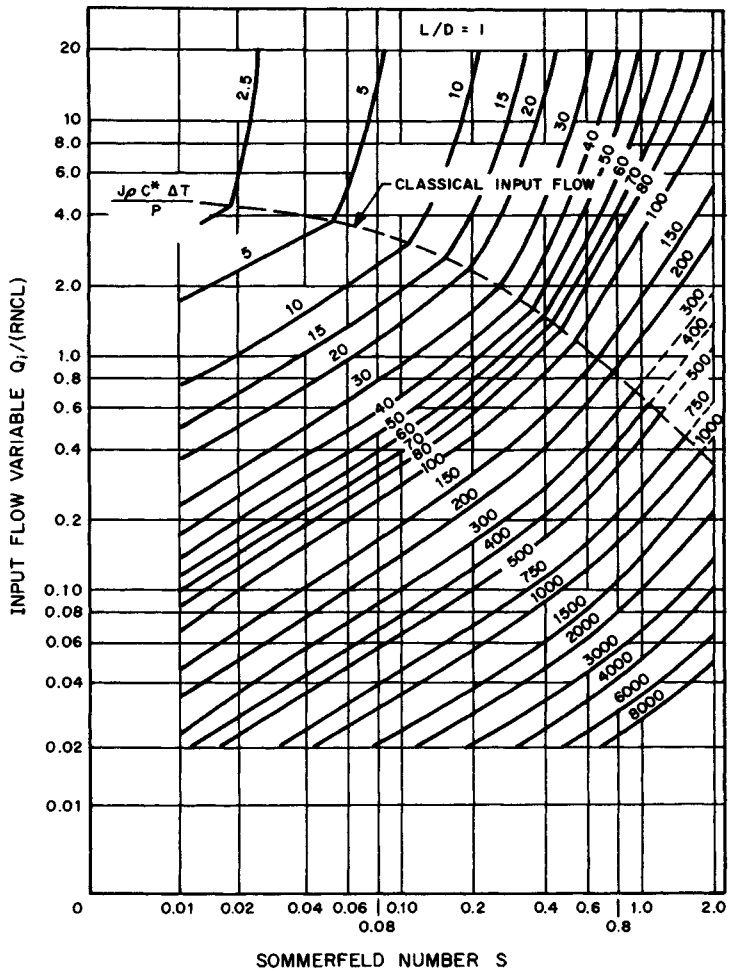

FIGURE 19.16 Inlet flow variable versus Sommerfeld number for parametric values of temperature-rise variable; $L/D = 1$, full journal bearing. *(From Connors [19.9].)*

For $Q_i/(RCNL) = 1$, the following sets of data were obtained by performing this calculation procedure:

$$\mu = \begin{cases} 1.5 \times 10^{-6} \text{ reyn} \\ 3.0 \times 10^{-6} \text{ reyn} \\ 6.0 \times 10^{-6} \text{ reyn} \end{cases} \qquad S = \begin{cases} 0.12 \\ 0.24 \\ 0.48 \end{cases}$$

$$\frac{J\rho C^*(T_a - T_i)}{P} = \begin{cases} 32 \\ 60 \\ 115 \end{cases} \qquad T_a = \begin{cases} 126.8°\text{F} \\ 150.2°\text{F} \\ 196.2°\text{F} \end{cases}$$

Using these and the lubricant μ versus T relation as presented in Table 19.16, we find the operating point to be

$$T_a = 155°\text{F} \qquad \mu = 3.2 \times 10^{-6} \text{ reyn}$$

Hence, $S = 0.256$. Also from Fig.19.14 we obtain $h_0/C = 0.52$, and so $h_0 = 0.00208$. Further, from Fig. 19.15, $(R/C)(f) = 5$, and so $f = 0.01$, which allows us to calculate the power loss to be 0.857 horsepower (hp). Assuming other values of $Q_i/(RCNL)$ permits Fig. 19.17 to be drawn. The Raimondi-Boyd value corresponding to $Q_i \to \infty$ is also presented.

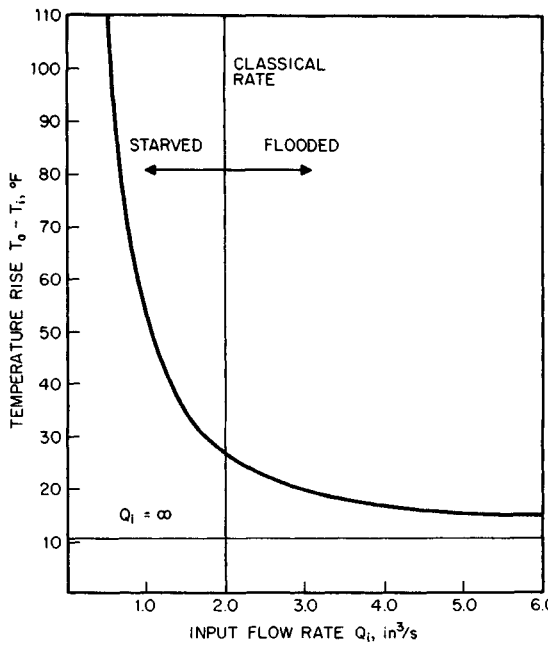

FIGURE 19.17 Lubricant temperature rise versus lubricant input flow rate (Example 3).

In Sec. 19.5.4 it was shown that

$$(T_a - T_i)_{\text{conduction}} = (1 - \lambda)(T_a - T_i)_{\text{no conduction}}$$

where λ = ratio of heat conduction to heat generation rate and is assumed to be a constant. By using this idea, a new operating point for a given $Q_i/(RCNL)$ can be determined. For example, with $\lambda = 0.25$ and $Q_i/(RCNL) = 1$, we find that $T_a = 147°\text{F}$, $h_0 = 0.0023$, and HP = 0.960 hp.

19.6.3 Optimization

In designing a journal bearing, a choice must be made among several potential designs for the particular application. Thus the designer must establish an optimum design criterion for the bearing. The design criterion describes the designer's objective, and numerous criteria can be envisioned (e.g., minimizing frictional loss, minimizing the lubricant temperature rise, minimizing the lubricant supply to the bearing, and so forth).

The search for an optimum bearing design is best conducted with the aid of a computer. However, optimum bearing design can also be achieved graphically. Moes and Bosma [19.10] developed a design chart for the full journal bearing which enables the designer to select optimum bearing dimensions. This chart is constructed in terms of two dimensionless groups called X and Y here. The groups include two quantities of primary importance to the bearing designer: minimum film thickness h_0 and frictional torque M_j; the groups do not contain the bearing clearance. The dimensionless groups are

$$X \equiv \frac{h_0}{R}\left(\frac{P}{2\pi N\mu}\right)^{1/2} \qquad Y \equiv \frac{M_j}{WR}\left(\frac{P}{2\pi N\mu}\right)^{1/2} \tag{19.15}$$

Both X and Y can be written in terms of the Sommerfeld number. Recalling that $h_0 = C(1-\varepsilon)$ and $S = (\mu N/P)(R/C)^2$, we can easily show that

$$X = \frac{1-\varepsilon}{\sqrt{2\pi S}} \qquad \text{and} \qquad Y = \frac{M_j}{WC}\frac{1}{\sqrt{2\pi S}}$$

Figure 19.18 is a plot of full journal bearing design data on the XY plane. In the diagram, two families of curves can be distinguished: curves of constant L/D ratio and curves of constant ε. Use of this diagram permits rather complicated optimization procedures to be performed.

Example 4. Calculate the permissible range of minimum film thickness and bearing clearance that will produce minimum shaft torque for a full journal bearing operating under the following conditions:

$\mu = 5 \times 10^{-6}$ reyn $\qquad D = 4$ in

$N = 1800$ rev/min $\qquad L = 3$ in

$W = 1800$ lbf

Solution. As a first step, we calculate the largest h_0 for the given conditions. This is easily accomplished by locating the coordinates on Fig. 19.18 corresponding to the maximum X for $L/D = \frac{3}{4}$, or

$$\begin{Bmatrix} X \\ Y \\ \varepsilon \end{Bmatrix} = \begin{Bmatrix} 0.385 \\ 4.0 \\ 0.54 \end{Bmatrix} \qquad \text{at } X = X_{\max}$$

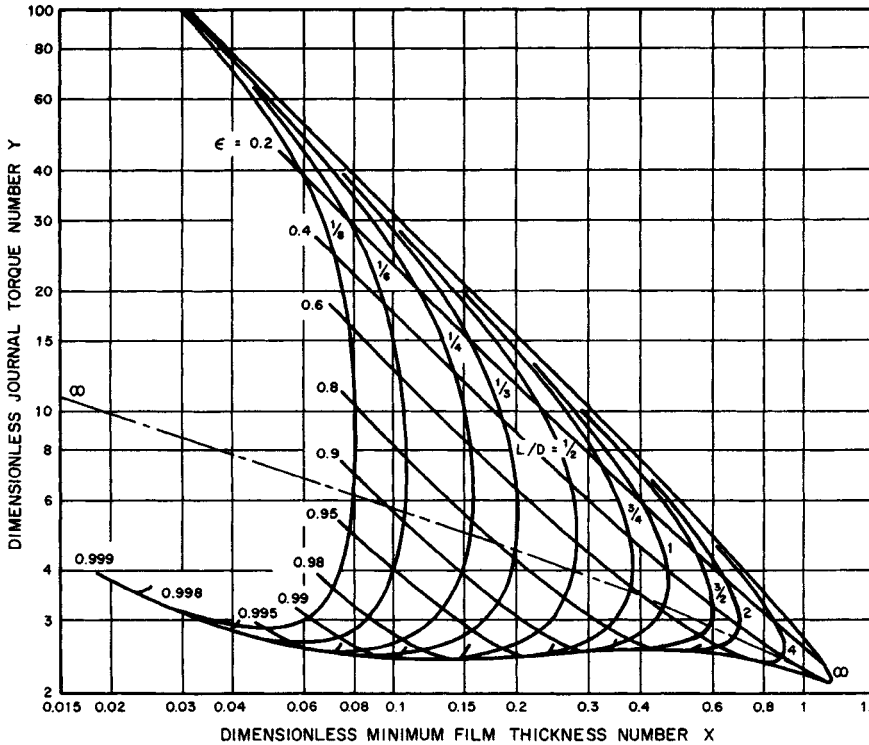

FIGURE 19.18 Optimization chart for full journal bearings. *(From Moes and Bosma [19.10].)*

Thus, from Eq. (19.15),

$$h_0 = 1.93 \times 10^{-3} \text{ in} \qquad \text{and} \qquad M_j = 36.1 \text{ in} \cdot \text{lbf}$$

The clearance is calculated from $C = h_0/(1 - \varepsilon) = 4.2 \times 10^{-3}$ in.

Next the coordinates on Fig. 19.18 corresponding to the minimum shaft torque (minimum value of Y at $L/D = \frac{3}{4}$) are located at

$$\begin{Bmatrix} X \\ Y \\ \varepsilon \end{Bmatrix} = \begin{Bmatrix} 0.18 \\ 2.5 \\ 0.97 \end{Bmatrix} \qquad \text{at } Y = Y_{\min}$$

Thus, from Eq. (19.15),

$$h_0 = 9.02 \times 10^{-4} \text{ in} \qquad \text{and} \qquad M_j = 22.6 \text{ in} \cdot \text{lbf}$$

The clearance for this case is calculated to be 3.01×10^{-2} in.

Thus the two optima (largest film thickness and smallest shaft torque) do not coincide. Thus, a compromise clearance value must generally be selected. Figure 19.19 is a plot of recommended minimum clearance for given shaft speed and diameter, which can be used as a helpful guide in this process.

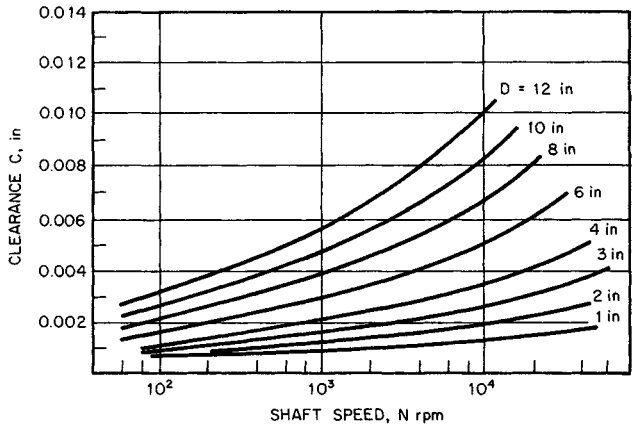

FIGURE 19.19 Recommended minimum clearance versus journal speed for a given journal diameter.

Example 5. Determine the bearing length and clearance for a full journal bearing operating steadily with minimum friction loss for the following conditions:

$\mu = 17.83 \times 10^{-6}$ $W = 1500$ lbf

$N = 4800$ rev/min $D = 6$ in

and a minimum allowable film thickness of

$$(h_0)_{\min} = 4.4 \times 10^{-4}$$

Solution. Because both X and Y contain the bearing length L, a new set of dimensionless groups not containing L must be developed. This pair is easily seen to be

$$U = (X)\left(\frac{L}{D}\right)^{1/2} = \frac{h_0}{R}\left(\frac{W}{2\pi\mu N D^2}\right)^{1/2} \tag{19.16}$$

$$V = (Y)\left(\frac{L}{D}\right)^{1/2} = \frac{M_j}{WR}\left(\frac{W}{2\pi\mu N D^2}\right)^{1/2} \tag{19.17}$$

For the given information, the smallest value of U (termed $U_{\min}$ because the smallest value of h_0 is used) can be directly calculated from Eq. (19.16):

$$U_{\min} = 0.10 \qquad \text{Thus,} \qquad X \geq (0.10)\left(\frac{D}{L}\right)^{1/2}$$

Selected L/D values permit an array of X values to be calculated. This in turn permits the minimum values of Y (that is, $Y_{\min}$) to be read from Fig. 19.18. Then corresponding $V_{\min}$ values can be calculated from Eq. (19.17). Table 19.17 contains the results of this operation.

TABLE 19.17 Summary of Calculated Results for Example 5

L/D	X	$Y_{\min}$	$V_{\min}$
1/4	0.2	No solution	
1/3	0.173	3.20	1.85
1/2	0.414	2.43	1.72
3/4	0.115	2.40	2.08
1	0.100	2.40	2.40

Next a cubic equation is fitted to the $V_{\min}$ data, and we find

$$V_{\min} = 4.057 - 11.927\frac{L}{D} + 18.742\left(\frac{L}{D}\right)^2 - 8.472\left(\frac{L}{D}\right)^3 \qquad (19.18)$$

The optimum value of L/D for a minimum friction loss can be found by differentiation, which yields the optimum bearing length:

$$L = 0.464D = 2.78 \text{ in}$$

The frictional loss can be calculated by inserting the optimum L/D ratio in the cubic equation:

$$V_{\min} = (Y)\left(\frac{L}{D}\right)^{1/2} = 1.712$$

Thus, $Y = 2.513$, and the eccentricity ratio is read from Fig. 19.18 as $\varepsilon \cong 0.98$. Finally the optimum bearing clearance is calculated to be $C = 2.2 \times 10^{-2}$ in.

19.7 GAS-LUBRICATED JOURNAL BEARINGS

Gas-lubricated journal bearings have been employed in a wide variety of modern industrial applications. For example, they are used in dental drills, high-speed machine tools, digital-computer peripheral devices, high-speed turbomachines, and navigational instruments.

Gas bearings produce very little friction even at high speeds; hence, they have low frictional losses and generate minimal amounts of heat. In addition, gas lubri-

cants are chemically very stable over a wide range of temperatures; they neither freeze nor boil; they are nonflammable; and they do not contaminate bearing surfaces. Gas bearings also have low noise characteristics.

On the negative side, gas bearings do not have much load-carrying capacity and have large startup wear. Also, because the gas film thickness is quite small, gas bearings require superior surface finish and manufacture. Great care must be exercised with the journal alignment. Further, thin films offer very little cushion or damping capacity; consequently, gas bearings are prone to certain vibrational instabilities.

19.7.1 Limiting Gas Bearing Solutions

The compressible-flow Reynolds equation, Eq. (19.7), is too complex to permit a general analytical solution, and numerical methods have been used to obtain gas bearing information. However, considerable insight can be gained by considering solutions for limiting cases. Besides the limiting geometric problems of long and short bearings, two other limiting classes of problems are important: gas films with low bearing numbers and gas films with high bearing numbers. The former pertain to low-speed, high-loading applications, and the latter pertain to very-high-speed, light-loading applications. Some bearing performance parameters for gas films with low and high bearing numbers are shown in Table 19.18.

TABLE 19.18 Long Gas Journal Bearing Performance Parameters, Limiting Cases, Long-Bearing Theory

Performance parameter	Low bearing number	Large bearing number
$\frac{p}{p_a}$	$\frac{1 + \Lambda\varepsilon \sin\theta(2 + \varepsilon\cos\theta)}{(2+\varepsilon)^2(1+\varepsilon\cos\theta)^2}$	$\frac{\sqrt{1 + 3\varepsilon^2/2}}{1 + \varepsilon\cos\theta}$
$\frac{W_R}{p_a DL}$	0	$\frac{\pi}{2}\left(1 + \frac{3\varepsilon^2}{2}\right)^{1/2}[(1-\varepsilon^2)^{-1/2} - 1]$
$\frac{W_T}{p_a DL}$	$\frac{\pi\varepsilon\Lambda}{(2+\varepsilon^2)\sqrt{1-\varepsilon^2}}$	0
ϕ	$\frac{\pi}{2}$	0
$\frac{F_j}{\mu UL}\frac{C}{R}$	$\frac{4\pi(1+2\varepsilon^2)}{(2+\varepsilon^2)\sqrt{1-\varepsilon^2}}$	$\frac{2\pi}{\sqrt{1-\varepsilon^2}}$
$\left(\frac{R}{C}\right)(f)$	$\frac{1+2\varepsilon^2}{3\varepsilon}$	$\frac{2\mu UR}{C^2 P_a\sqrt{(1+3\varepsilon^2/2}(1-\sqrt{1-\varepsilon^2})}$

19.7.2 Stability Considerations

The journal bearing of a rotating machine cannot be treated separately. It is part of a complex dynamic system, and its design can influence the dynamic behavior of the entire system. Bearing damping controls vibration amplitude and tolerance to any imbalance and, to a large extent, determines whether the rotor will be dynamically stable. A bearing running in an unstable mode can lose its ability to support load, and rubbing contact can occur between the bearing and the shaft surfaces.

Rotor bearing instabilities are particularly troublesome in gas-lubricated bearings; the film is considerably thinner in gas bearings than in liquid-lubricated bearings and so does not possess the damping capacity. We can differentiate between two forms of dynamic instability: *synchronous whirl* and *half-frequency whirl* (also called fractional-frequency whirl and film whirl).

Synchronous Whirl. A rotating shaft experiences periodic deflection (forced vibration) because of the distribution of load, the method of shaft support, the degree of flexibility of the shaft, and any imbalance within the rotating mass. This deflection causes the journal to orbit within its bearings at the rotational speed. When the frequency of this vibration occurs at the natural frequency (or critical speed) of the system, a resonance condition exists. In this condition, the amplitude of vibration (size of the journal orbit) increases and can cause bearing failure. Because the shaft rotational speed and the critical speed coincide, this form of instability is termed *synchronous whirl.*

Since stable operation occurs on either side of the critical speed, the bearing system must be designed so that critical speeds do not exist in the operating speed range. This can be accomplished by making the critical speeds either very large or very small. Large critical speeds can be established by increasing the bearing stiffness by reducing the bearing clearance. Lower critical speeds can be established by increasing the shaft flexibility. The instability can also be suppressed by mounting the bearing in a flexible housing which introduces additional system damping.

Half-Frequency Whirl. A deflected rotating shaft has its center whirl, or orbit, around the center of the bearing. When the whirl speed Ω is equal to or somewhat less than half the rotational speed of the shaft, ω, the hydrodynamic capacity of the bearing to support a load is diminished and, in fact, may fall to zero. With any subsequent rotational speed increase, the whirl amplitude will increase, and the bearing and journal may come into violent contact. This form of self-activated vibrational instability is called *half-frequency* or *half-speed whirl.* Because the whirl speed for gas bearings is generally less than the rotational speed, the instability is also termed *fractional-frequency whirl.* Figure 19.20 is a map for assessing the stability of a full journal bearing.

Half-speed whirl may be suppressed by altering the circumferential symmetry of the bearing. This can be accomplished by providing axial grooves in the bearing surface, by dividing the circumference into a number of sections, or lobes, or by using tilting pads. Also, introducing more damping into the system through the use of flexible housing mounts can be helpful.

19.7.3 Cylindrical Ungrooved Gas Journal Bearings

Complete plain cylindrical journal bearings are generally used in applications that require support of a fixed, unidirectional load. Self-excited whirl instability is a com-

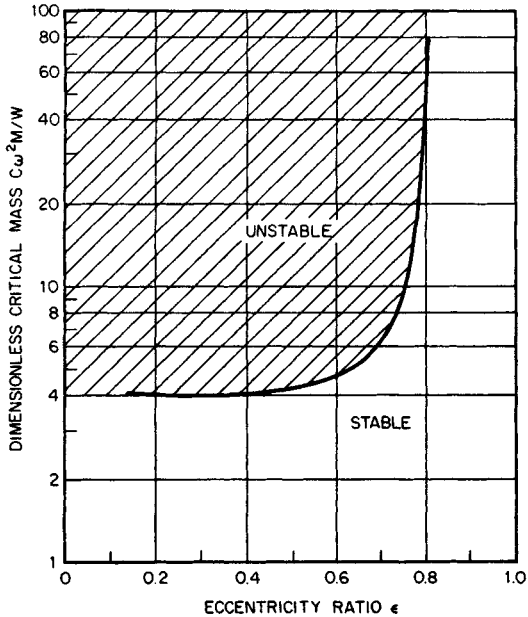

FIGURE 19.20 Bearing stability for full journal bearing, $L/D = 1$.

mon problem with high-speed rotor systems supported by this type of bearing. However, if the load is sufficiently large to have an eccentricity ratio on the order of 0.8, whirl problems are reduced (refer to Fig. 19.20).

Ungrooved cylindrical gas bearings have been analyzed by Raimondi [19.11]. Performance characteristics were developed numerically and presented in the form of various design charts for L/D ratios of ½, 1, and 2. Figures 19.21 to 19.23 are a sampling of these charts for an L/D ratio of 1.

A porous journal bearing is a plain cylindrical journal bearing with a porous liner that is fixed in the bearing housing (Fig. 19.24). An externally pressurized gas is supplied to the outer surface of the liner and flows through the porous material into the bearing clearance space.

The steady performance of a self-acting porous gas bearing of finite length has been determined by Wu [19.12]. Table 19.19 shows a sample of these performance data. The data are applicable for a particular porous linear thickness ratio (0.083) and for particular combinations of the *slip coefficient* α (dependent on the structure of the porous material), the *permeability* k (a physical property of the porous material), and bearing dimensions R and C.

Example 6. For the following conditions

$D = 0.5$ in	$N = 47\,000$ rev/min
$L = 0.5$ in	$\mu = 2.6 \times 10^{-9}$ reyn (air at 80°F)
$C = 2 \times 10^{-4}$ in	$p_a = 40$ psi
	$W = 6.1$ lbf

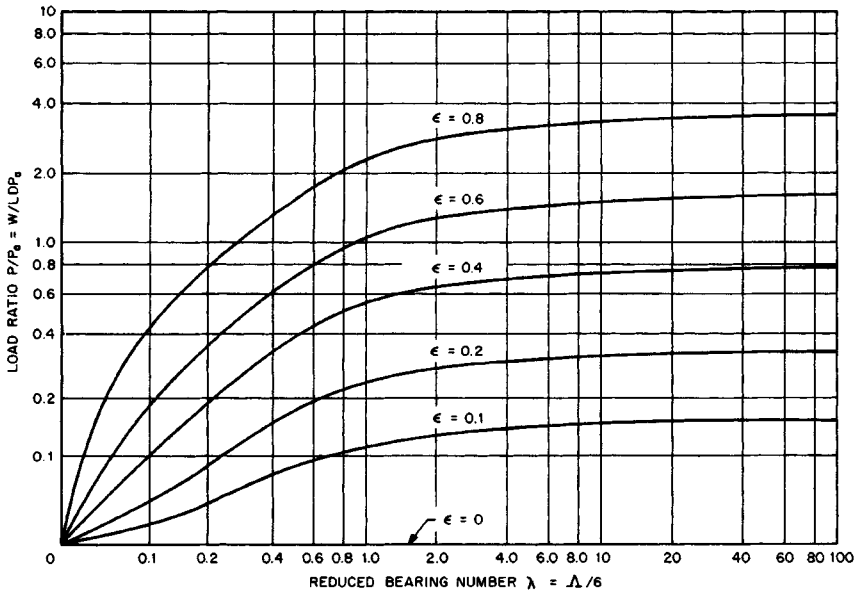

FIGURE 19.21 Load ratio versus reduced bearing number of an ungrooved cylindrical gas bearing; $L/D = 1$. *(From Raimondi [19.11].)*

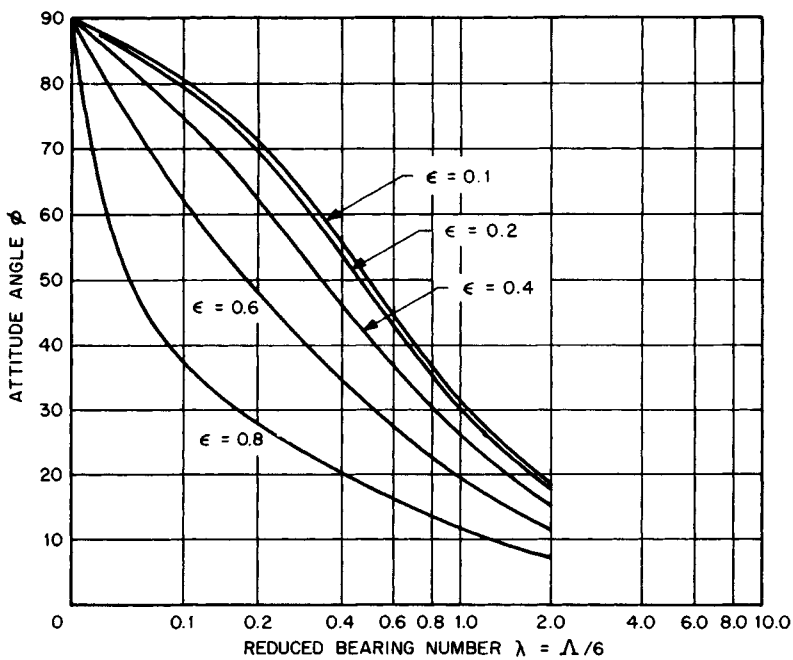

FIGURE 19.22 Attitude angle versus reduced bearing number of an ungrooved cylindrical gas bearing; $L/D = 1$. *(From Raimondi [19.11].)*

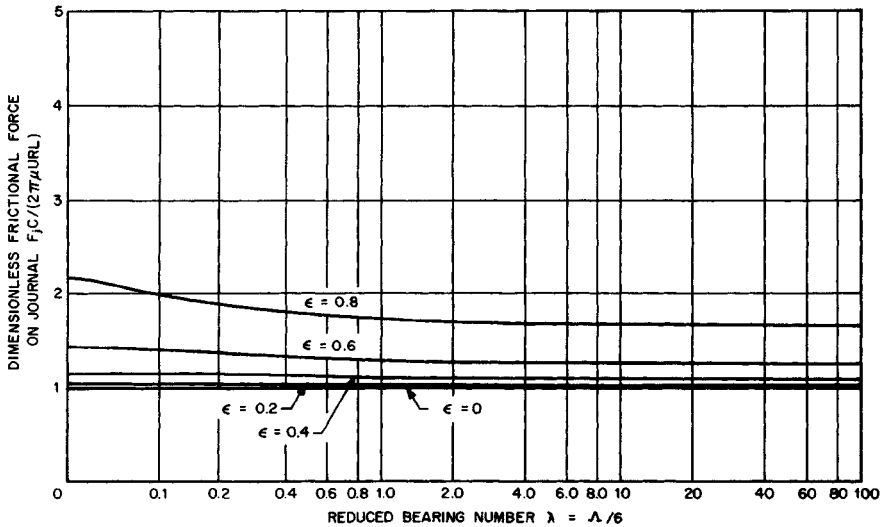

FIGURE 19.23 Dimensionless journal frictional force versus reduced bearing number of an ungrooved cylindrical gas bearing; $L/D = 1$. *(From Raimondi [19.11].)*

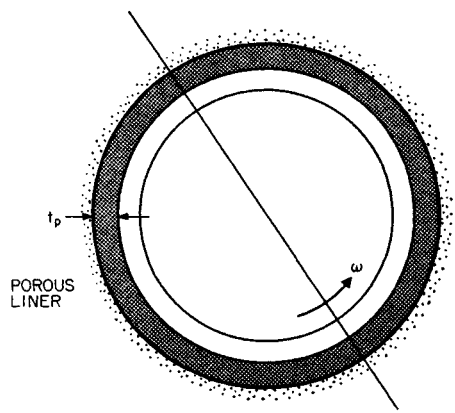

FIGURE 19.24 Porous journal bearing.

compare the performance of a porous gas bearing to that of a solid wall bearing. The porous bearing material is ceramic 0.021 in thick with a permeability $k = 1.33 \times 10^{-12}$ in^2 and a slip coefficient $\alpha = 0.3$.

Solution. Since $L/D = 1$, $t_p/R \cong 0.083$, $\beta = \alpha C/k \cong 50$, and $\Omega = 12kR/C^3 \cong 0.5$, the data of Table 19.19 may be used. The bearing number is

$$\Lambda = \frac{6\mu\omega}{p_a}\left(\frac{R}{C}\right)^2 = 3.0$$

TABLE 19.19 Gas-Lubricated Bearing Performance Data, $L/D = 1$, $t_p/R = 0.083$, $\Omega = 0.5$, $\beta = 50$

ε	Λ	$\frac{P}{p_a}$	ϕ, deg	$\left(\frac{R}{C}\right)(f)$
0.2	0.6	0.039	80.563	8.1034
	1.2	0.0756	72.109	8.3784
	3.0	0.1594	52.470	9.9199
	6.0	0.2272	34.402	13.8773
	12.0	0.2662	20.290	23.6302
	50.0	0.2959	7.602	88.4725
	100.0	0.3054	5.014	171.9223
	∞	0.3264	0	∞
0.4	0.6	0.0853	77.245	4.0835
	1.2	0.1638	66.670	4.2517
	3.0	0.3441	46.382	5.0012
	6.0	0.5067	30.262	6.7025
	12.0	0.6164	17.806	10.9197
	50.0	0.6982	6.424	39.9776
	100.0	0.7188	4.164	77.6340
	∞	0.7746	0	∞
0.6	0.6	0.1500	70.129	2.8072
	1.2	0.2872	56.903	2.8961
	3.0	0.6102	37.598	3.3003
	6.0	0.9322	24.537	4.2078
	12.0	1.1854	14.488	6.4992
	50.0	1.3774	4.962	23.0667
	100.0	1.4186	3.122	44.7611
	∞	1.5603	0	∞
0.8	0.6	0.2547	61.657	2.2908
	1.2	0.4995	47.468	2.2971
	3.0	1.1050	31.147	2.4980
	6.0	1.7837	20.348	2.9210
	12.0	2.3907	12.272	4.2374
	50.0	2.8736	4.046	14.4249
	100.0	2.9640	2.436	27.9331
	∞	3.4193	0	∞

SOURCE: Ref. [19.12].

The load ratio is

$$\frac{P}{p_a} = \frac{W/(LD)}{p_a} = 0.61$$

Entering Table 19.18 with these values, we find

$$\varepsilon = 0.6 \qquad \phi = 37.598 \qquad \left(\frac{R}{C}\right)(f) = 3.3003$$

For the same values we can find from Figs. 19.21 to 19.23 for the solid wall bearing $\varepsilon = 0.54$, $\phi = 33.7°$, and

$$\frac{F_j C}{2\pi\mu URL} = 1.18$$

From the last value, we may compute for comparative purposes

$$\left(\frac{R}{C}\right)(f) = 3.038$$

Thus the porous bearing operates at a larger eccentricity ratio (which indicates better stability) but has larger frictional loss. On the other hand, for a given ε, the porous bearing has a lower load capacity compared to the solid wall bearing. This loss of load capacity becomes more severe as the eccentricity ratio is increased.

19.7.4 Axially Grooved Gas Journal Bearings

The addition of axial slots, or grooves, in the bearing surface can produce several positive effects. Feed grooves can reduce frictional heating and energy losses. The grooves, in effect, turn the surface into a number of partial arc bearings, which can reduce the tendency for half-frequency whirl instability. What is more, grooving a bearing leads to only a slight increase in the manufacturing costs. Although a variety of grooving arrangements can be envisioned, three or four equally spaced axial grooves are typically employed. Feed grooves of 30° to 60° extent are commonly used. However, bearing stability decreases with increase in the groove size.

Castelli and Pirvics [19.13] presented tabular design data for axially grooved gas bearings. The subtended angle of each groove was taken to be 5°. Figures 19.25 and 19.26 are sample design chart data for a gas bearing with three grooves and an *L/D* ratio of 2.

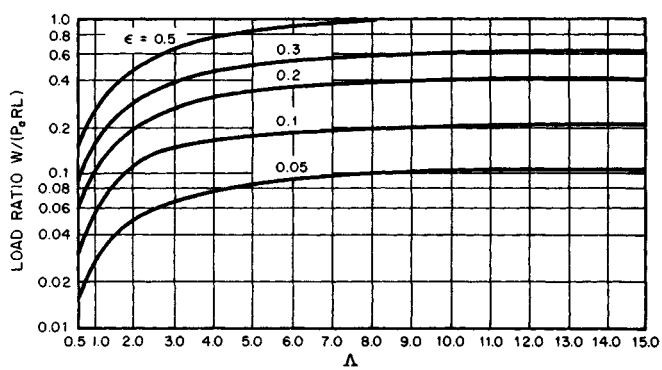

FIGURE 19.25 Load ratio versus compressibility number for an axial-groove gas bearing, *L/D* = 2; three evenly spaced axial grooves—first groove 60° clockwise from load line. *(From Castelli and Pirvics [19.13].)*

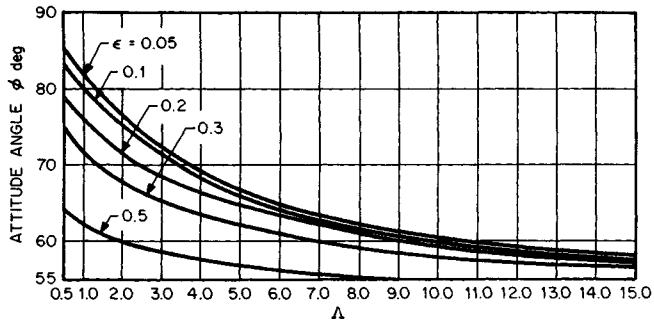

FIGURE 19.26 Attitude angle versus compressibility number for an axial-groove gas bearing, $L/D = 2$; three evenly spaced axial grooves—first groove 60° clockwise from load line. *(From Castelli and Pirvics [19.13].)*

19.7.5 Noncircular Gas Journal Bearings

For low eccentricity ratios, a noncircular gas bearing has superior stability properties but inferior load capacity when it is compared with a circular gas bearing. At higher eccentricity ratios, the load-carrying capacity of the noncircular gas bearing exceeds that of the circular gas bearing. For applications where load capacity is not an issue (e.g., in vertical-shaft cases), use of a noncircular gas bearing minimizes stability concerns that exist at the lower eccentricity ratios.

Pinkus [19.14] has investigated the performance of elliptical and three-lobe gas bearings. It was found that the direction of load application is important to the performance of a noncircular gas bearing. In fact, load-carrying capacity can be optimized by rotating the bearing relative to the load line. The rotation is generally clockwise anywhere from a few degrees to 25°. Table 19.20 presents a comparison of expected eccentricity ratios for given values of S and Λ for circular, elliptical, and three-lobe gas bearings. Higher values of ε required by the noncircular bearings over the ε for the circular bearing at the same Sommerfeld number indicate a lower load capacity. Pinkus also presented envelopes of operation. Figure 19.27 is a plot of Som-

TABLE 19.20 Eccentricity Ratio versus Sommerfeld and Bearing Numbers for Circular, Elliptical, and Three-Lobe Noncircular Gas Bearings

Bearing number Λ	Sommerfeld number S	Eccentricity ratio ε				
		Circular	Elliptical central loading	Elliptical optimum loading	Three-lobe central loading	Three-lobe optimum loading
1	0.365	0.2	0.54	0.525	0.55	0.545
1	0.162	0.4	0.59	0.56	0.615	0.605
1	0.0866	0.6	0.67	0.635	0.70	0.685
1	0.0381	0.8	0.815	0.77	0.84	0.815
3	0.365	0.25	0.57	0.535	0.595	0.57
3	0.162	0.475	0.65	0.59	0.68	0.645
3	0.0860	0.655	0.75	0.685	0.80	0.755

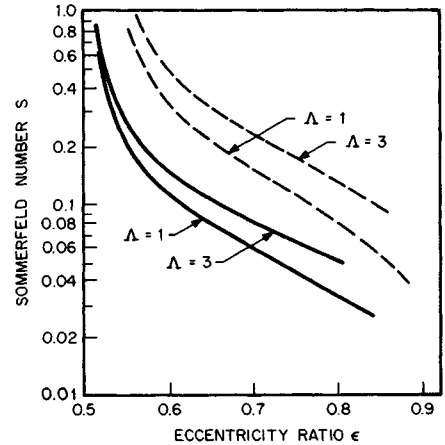

FIGURE 19.27 Sommerfeld number versus eccentricity ratio for a noncentrally loaded elliptical gas bearing, $L/D = 1$. *(From Pinkus [19.14].)*

merfeld number versus the eccentricity ratio for a noncentrally loaded elliptical gas bearing. The upper set of curves represents the largest ε for a given S at a particular Λ, and it would be used in an attempt to avoid stability problems. The lower set of curves represents the optimum loading conditions.

19.8 HYDROSTATIC JOURNAL BEARING DESIGN

Hydrostatic journal bearings (also called *externally pressurized* bearings) offer large radial load-carrying capacities at all rotational speeds (including zero). They exert very little friction and have controllable stiffness. The principal disadvantage of hydrostatic journal bearings is the cost of the pressurized lubricant supply system. These bearings are widely used in the machine-tool industry.

19.8.1 Classification of Bearings and Components

There are basically three types of hydrostatic journal bearings: the single-pad, the multipad, and the multirecess. The various types are depicted in Table 19.21.

The main components of a hydrostatic journal bearing are the pad and the lubricant supply system. The pad consists of a recess, or pocket, region and the surrounding land material. The recess is generally deep compared with the film thickness: typically the depth is taken to be 20 times the radial clearance. In sizing the recess, the land width is reduced as much as practical; however, if the land width is too small, edge effects can become significant. These effects can be avoided if the land width is taken to be greater than 100 times the clearance.

Pressurized lubricant is provided to each bearing recess through the supply system. This system may be as simple as a direct line between the recess and the supply pump. Bearings using such simple systems are termed *noncompensated hydrostatic*

TABLE 19.21 Types of Hydrostatic Journal Bearings

Type		Comments
Single-pad journal bearing		1. Included angle less than 180°. 2. Normally used to support unidirectional loads. 3. May have multiple recesses. 4. Lubricant flow and pad design based on a maximum load applied to a uniform film equaling minimum radial clearance $R_B - R_J$.
Multipad journal bearing	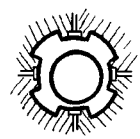	1. Included angle of each pad is less than 180°. 2. Used for rotating, oscillating, or reversing radial loads. 3. Two opposed pads can be used for reversing loads. 4. If angular variation of the load is less than 80°, a two-pad journal bearing may be used. 5. Bearing stiffness is reduced if load is directed between pads. 6. Axial grooves provide cooling capability at high rotational speeds.
Multirecess journal bearing	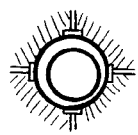	1. No pressure-reducing grooves between recesses. 2. Usually contains four or more recesses. 3. Used for rotating and reversing loads. 4. Does not require as much flow per recess as multipad type. 5. Circumferential flow from high-pressure pockets to lower-pressure pockets evens pressure distribution around bearing.

bearings and are frequently used to lift highly loaded journals prior to rotation. In that context they are termed *oil lifts.*

In order for a single pump to deliver lubricant to more than one pad or recess, restrictors (or compensating devices) are required in each supply line. Restrictors limit the flow to each pad, thereby permitting all pads to become activated. Without compensating devices, pad imbalance would occur. Restrictors, then, are used to control the operation of a hydrostatic bearing.

There are three common types of restrictors: the capillary tube, the orifice plate, and the flow control valve. Table 19.22 compares these devices. This table was pre-

pared from a comprehensive series of papers on hydrostatic bearing design by Rippel [19.15]. In addition to flow-load control, the resistor affects the stiffness of the bearing. Bearing stiffness is related to the ability of the bearing to tolerate any changes in the applied load.

19.8.2 Design Parameters

For hydrostatic journal bearings at low rotational speeds, the primary design parameters are maximum load, lubricant flow rate, and stiffness. Of secondary importance are considerations of frictional horsepower and lubricant temperature rise.

The load-carrying capacity of a hydrostatic journal bearing is generally written as

$$W = a_f A_p p_r \tag{19.19}$$

where a_f = pad load coefficient, A_p = projected bearing area, and p_r = recess pressure. The pad load coefficient is dimensionless and physically represents the ratio of the average lubricant pressure in the pad to the lubricant pressure supplied to the pad. O'Donoghue and Rowe [19.16] give equations for a_f for both multirecess and multipad bearings.

The lubricant flow rate may be determined from

$$Q = q_f \frac{h^3 p_r}{\mu} \tag{19.20}$$

where q_f = flow factor for a single pad. The flow factor depends on the geometry and land widths of the bearing.

Journal bearing stiffness expresses the ability of the bearing to accommodate any changes in the applied load. Stiffness is proportional to the slope of the bearing load versus film thickness curve, or

$$s = -\frac{dW}{dh} \tag{19.21}$$

Stiffness will depend on the method of flow control (capillary tube, etc.) and the amount of circumferential flow. O'Donoghue and Rowe [19.16] provide a detailed derivation of the journal bearing stiffness and have developed equations for both multipad and multirecess bearings.

19.8.3 Design Procedures

A variety of design procedures are available for hydrostatic bearings. Some are based on experimental findings, whereas others are based on numerical solutions of the Reynolds equation.

Many existing methods incorporate numerous charts and tables which clearly place a limit on the methods; in order to use these procedures, the appropriate reference must be consulted. Alternatively, O'Donoghue and Rowe [19.16] have developed a general approximate method of design that does not require the use of various design charts. The method is strictly valid for thin land bearings, and many of the parameters are conservatively estimated. The following is a condensation of this design procedure for a multirecess bearing:

TABLE 19.22 Comparison of Three Types of Flow Resistors

	Initial cost	Fabrication and installation costs	Reliability	Availability	Ability to remain unclogged	Serviceability	Life	Flow relationship	Restrictions	Notes
Capillary tube	4†	3	5	5	1	4	5	$Q = k_c \dfrac{P_s - P_r}{\mu}$ $k_c = \pi D_c^4/128L_c$	$L_c > 20D_c$ $R_e = \dfrac{4\rho Q}{\pi D_c \mu} < 2000$	1. Laminar flow device. 2. Hypodermic needle tubing can generally be used. 3. To prevent clogging $D_c > 0.025$ in.
Sharp-edged orifice	5	2	5	5	3	4	4	$Q = k_0(P_s - P_r)^{1/2}$ $k_0 = \dfrac{C_D \pi D_0^2}{2\sqrt{2\rho}}$	$C_D = f(R_e)$ $R_e = \dfrac{\sqrt{2\rho(P_s - P_r)}D_0}{\mu}$ $C_D \sim 0.6$ for $R_e > 15$ and $D_0/D_{\text{line}} < 0.1$	1. Turbulent flow device. 2. To prevent clogging, $D_0 > 0.020$ in.
Flow control valve	1	4	2	5	5	2	2	$Q = k_v$ k_v = constant		1. Relatively expensive. 2. Flow is maintained at constant value.

†Rating numbers: 5 is high (best); 1 is low (worst).

Design Specification

1. Set the maximum load W.
2. Select the number of recesses n (typically $n = 4$, but $n = 6$ for high-precision bearings).
3. Select a pressure ratio p_r/p_s (a design value of 0.5 is recommended).

Bearing Dimensions

1. Calculate the bearing diameter $D = \sqrt{W/50}$ in.
2. Set width $L = D$.
3. Calculate the axial-flow land width a (refer to Fig. 19.28; recommended value: $a = L/4$).

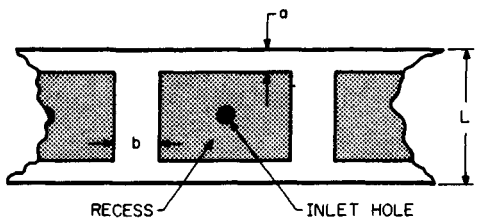

FIGURE 19.28 Hydrostatic pad geometry.

4. Calculate the circumferential land width b [refer to Fig. 19.28; recommended value: $b = \pi D/(4n)$].
5. Calculate the projected pad area $A_p = D(L - a)$.
6. Calculate the recess area for one pad only: $A_r = (\pi D - nb)(L - a)/n$.
7. Calculate the effective frictional area: $A_f = (\pi DL/n) - 0.75A_f$.

Miscellaneous Coefficients and Parameters

1. Establish a design value of film thickness h_d (recommended value: 50 to 10 times larger than the machinery tolerance on h).
2. Calculate the circumferential flow factor $\gamma = na(L - a)/(\pi Db)$; for recommended values of D, L, a, and b: $\gamma = \frac{3}{4}(n/\pi)^2$.
3. Compute the design dimensionless stiffness parameter $\bar{s}$ from Table 19.23 depending on the method of flow control selected.
4. Calculate the flow factor $q_f = \pi D/(6an)$.

Performance Parameters

1. Calculate the minimum supply pressure $p_{s,\min} = 2W/(a_f A_p)$ [recommended: $a_f = \bar{s}$ (capillary tube at design Table 19.23)].

TABLE 19.23 Dimensionless Stiffness at Design Condition for Multirecess Bearing

$$\bar{s} = \frac{C_1}{1 + C_{2\gamma}}$$

Number of recesses n	Capillary tube		Sharp-edged orifice		Flow control valve		Recommended value of γ†
	C_1	C_2	C_1	C_2	C_1	C_2	
3	0.27	0.75	0.36	1.0	0.54	1.5	0.68
4	0.96	0.50	1.28	0.67	1.91	1.01	1.22
5	1.03	0.35	1.38	0.46	2.13	0.69	1.90
6	1.08	0.25	1.43	0.33	2.15	0.50	2.74

†SOURCE: Ref. [19.16].

2. Calculate the stiffness $s = p_s A_p \bar{s}/h_d$ (if this value is too low, either D and/or p_s must be increased).
3. Calculate the minimum running clearance $h_0 = h_d - W/s$.
4. Determine the flow rate $Q = (nq_f p_s h^3 d)/(2\mu)$. A calculated value of viscosity can be used:

$$\mu = \frac{60 P_s h^2 d \sqrt{q_f/(2A_f)}}{\pi D N} \quad \text{reyn}$$

REFERENCES

19.1 G. G. Hirs, "The Load Capacity and Stability Characteristics of Hydrodynamic Grooved Journal Bearings," *ASLE Transactions,* vol. 8, 1965, pp. 296–305.

19.2 E. R. Booser, "Plain-Bearing Materials," *Machine Design,* June 18, 1970 (bearings reference issue), pp. 14–20.

19.3 V. Hopkins, "Self-Lubricating Bearing Materials—A Review," *Assessment of Lubricant Technology,* ASME, 1972, pp. 21–26.

19.4 A. W. J. DeGee, "Selection of Materials for Lubricated Journal Bearings," *Wear,* vol. 36, 1976, pp. 33–61.

19.5 B. R. Reason and I. P. Narang, "Rapid Design and Performance Evaluation of Steady State Journal Bearings—A Technique Amendable to Programmable Hand Calculators," *ASLE Transactions,* vol. 25, no. 4, 1982, pp. 429–449.

19.6 J. Shigley and C. R. Mischke, *Mechanical Engineering Design,* 5th ed., McGraw-Hill, New York, 1989, pp. 498–507.

19.7 A. A. Raimondi and J. Boyd, "A Solution for the Finite Journal Bearing and Its Application to Analysis and Design," I, II, and III, *ASLE Transactions,* vol. 1, 1958, pp. 159–174, 175–193, and 194–209, respectively.

19.8 A. Seireg and S. Dandage, "Empirical Design Procedure for the Thermodynamic Behavior of Journal Bearings," *ASME Journal of Lubrication Technology,* vol. 104, April 1982, pp. 135–148.

19.9 H. J. Connors, "An Analysis of the Effect of Lubricant Supply Rate on the Performance of the 360° Journal Bearing," *ASLE Transactions,* vol. 5, 1962, pp. 404–417.

19.10 H. Moes and R. Bosma, "Design Charts for Optimum Bearing Configurations: 1—The Full Journal Bearing," *ASME Journal of Lubrication Technology,* vol. 93, April 1971, pp. 302–306.

19.11 A. A. Raimondi, "A Numerical Solution for the Gas Lubricated Full Journal Bearing of Finite Length," *ASLE Transactions,* vol. 4, 1961, pp. 131–155.

19.12 E. R. Wu, "Gas-Lubricated Porous Bearings of Finite Length—Self-Acting Journal Bearings," *ASME Journal of Lubrication Technology,* vol. 101, July 1979, pp. 338–348.

19.13 V. Castelli and J. Pirvics, "Equilibrium Characteristics of Axial-Grooved Gas-Lubricated Bearings," *ASME Journal of Lubrication Technology,* vol. 89, April 1967, pp. 177–196.

19.14 O. Pinkus, "Analysis of Noncircular Gas Journal Bearings," *ASME Journal of Lubrication Technology,* vol. 87, October 1975, pp. 616–619.

19.15 H. C. Rippel, "Design of Hydrostatic Bearings," *Machine Design,* parts 1 to 10, Aug. 1 to Dec. 5, 1963.

19.16 J. P. O'Donoghue and W. B. Rowe, "Hydrostatic Bearing Design," *Tribology,* vol. 2, February 1969, pp. 25–71.